

A holistic optimization framework for integrating PV systems into
building façades

by

Parnian Bakmohammadi

A thesis submitted in partial fulfillment of the requirements for the degree of

Master of Science

in

Civil (Cross-disciplinary)

Department of Civil and Environmental Engineering

University of Alberta

© Parnian Bakmohammadi, 2023

Abstract

In recent years, the growing concern over fossil fuel supply insecurity and its negative environmental impacts has led researchers to focus on advancing renewable energy technologies. Buildings, which account for a significant portion of global energy consumption, offer great potential for incorporating renewable energy applications. Solar energy, particularly through the installation of PV panels on building façades, is regarded as a promising resource. However, the full potential of PV systems in buildings has not always been maximized, highlighting the need for collaborative efforts to develop practical and optimized designs for PV integration.

This study presents a comprehensive framework that considers energy efficiency, economic viability, and environmental factors when integrating PV panels into building façades. The process begins with importing 3D models of buildings from Google Maps into Rhinoceros 3D software. After simplifying the building geometry, a deep learning model is used to identify areas suitable for PV installation, primarily the walls. PV generation and energy demand simulation models are then defined, and an evolutionary multi-objective optimization engine is utilized to determine the best PV system design parameters, including tilt, azimuth, and rotation angles, as well as the vertical and horizontal distances of the panels. This holistic approach allows engineers to thoroughly assess multiple sustainability aspects related to various PV system layouts and make informed decisions based on their preferences.

The framework is applied to two buildings situated in a cold climate on the North Campus of the University of Alberta in Edmonton, Alberta, Canada, serving as case study examples. The results demonstrate that adjusting the priorities of objectives can lead to different optimized solutions,

emphasizing the importance of considering various factors when designing PV systems for building façades.

Preface

The research presented in this thesis was carried out in partnership with Dr. Mustafa Gül's research team. This thesis, authored by Parnian Bakmohammadi, constitutes an entirely original contribution, with no prior publication of its content.

Dedication

I dedicate this research to all those who are committed to advancing the cause of sustainable buildings and cities, and to making our world a more environmentally responsible and resilient place for future generations.

Acknowledgment

I want to convey my heartfelt gratitude to Dr. Mustafa Gül, my supervisor, for his consistent guidance, unwavering support, and encouragement throughout this research. His dedicated time and expertise were instrumental in the successful completion of this thesis. I extend my thanks to my colleagues at the University of Alberta, Nima Narjabadifam, Dr. Maziar Jamshidi, and Asdrubal Cheng Chen for their valuable insights and steadfast support during my academic journey. Lastly, I am deeply appreciative of my parents and brothers for their enduring support, encouragement, and the wellspring of inspiration they provided throughout this research endeavor.

Table of Contents

<i>Chapter One: Introduction</i>	1
1.1 Problem Statement & Research Objectives	4
1.2 Thesis Structure	4
<i>Chapter Two: Literature Review</i>	6
2.1 PV Façade Systems.....	6
2.2 Optimizing PV Façade System Layout.....	8
2.3 Deep Learning for Façade Parsing.....	17
2.4 Research Gap, Scope & Novelty	21
<i>Chapter Three: Methodology</i>	24
3.1 Overview.....	24
3.2 Simplified Building Geometry.....	25
3.2.1 3D Models of Buildings.....	27
3.2.2 Building Footprints	30
3.2.3 Simplification & Recreation of Building Meshes.....	31
3.3 Façade Segmentation	35
3.3.1 Façade Segmentation Dataset	35
3.3.2 Deep Learning Model Development.....	38
3.4 Combining 2D Images with 3D Models	39
3.4.1 Rectification & Image Processing of Predicted Segmentation Masks.....	40

3.4.2	Projecting Processed Masks onto 3D Models.....	41
3.5	Optimization Framework.....	42
3.5.1	PV System Design Parameters.....	42
3.5.2	Power generation of PV system.....	46
3.5.3	Energy Simulation Model.....	49
3.5.4	Objective Functions.....	49
3.5.5	Multi-Objective Optimization of PV Layout.....	53
<i>Chapter Four: Results & Discussion.....</i>		<i>56</i>
4.1	Simplified Building Geometries.....	56
4.2	Façade Segmentation Results.....	57
4.2.1	CNN Model’s Training Results.....	58
4.2.2	Samples of Predicted Masks.....	60
4.3	Combined 2D Segmented Masks with 3D Models.....	62
4.3.1	Rectified & Processed Segmented Masks.....	62
4.3.2	Projected Mask onto Façades.....	64
4.4	Framework Validation.....	66
4.5	Optimization Results.....	67
4.5.1	CSC.....	67
4.5.2	NW-VVC.....	76
4.6	Adjusting the Significance of Sustainability Factors.....	80
4.7	Discussion & Recommendations.....	83

4.8	Limitations & Future Work	85
	<i>Chapter Five: Conclusion</i>	88
	<i>References</i>	91

List of Tables

Table 1. Details of "Façade Segmentation" dataset	36
Table 2. Class names and their corresponding label colors	36
Table 3. PV module specifications	44
Table 4. Estimated PV system losses (not including the snow loss factor) [84]	48
Table 5. Overview of the energy-related data pertaining to the life cycle of polycrystalline solar panels	53
Table 6. Performance evaluation of the segmentation model on the test set	60
Table 7. Settings of optimization algorithm	67
Table 8. PV design parameters for the south façade of CSC building	68
Table 9. PV design parameters for the west façade of CSC building	71
Table 10. PV design parameters for the east façade of CSC building	74
Table 11. PV design parameters for the south façade of NW-VVC	77
Table 12. PV design parameters for the west façade of NW-VVC	79
Table 13. PV system design parameters for the south façade of CSC building under different scenarios	81
Table 14. Achieved objective values for south façade of CSC building in various scenarios	81

List of Figures

Figure 1. Photovoltaic electricity potential of Canada (Canada source: https://solargis.com/maps-and-gis-data/download/canada , © 2020 The World Bank, Source: Global Solar Atlas 2.0, Solar resource data: Solargis).....	2
Figure 2. Examples of BIPV & BAPV applications: (a) rooftop BAPV application (Image capture: May 2023 ©2023 Google); (b) semitransparent BIPV for facade application at University of Alberta.....	7
Figure 3. (a) General overview of framework; (b) Detailed workflow of framework	26
Figure 4. Google’s 3D model of CSC (Imagery ©2023 Google, Imagery ©2023 CNES / Airbus, Maxar Technologies, Map data ©2023 Google)	28
Figure 5. Google’s 3D model of NW-VVC (Imagery ©2023 Google, Imagery ©2023 CNES / Airbus, Maxar Technologies, Map data ©2023 Google)	28
Figure 6. Captured Google’s 3D model in .rdc format using RenderDoc v1.25	29
Figure 7. Imported Google Maps Capture into Blender v3.4.1	29
Figure 8. Imported Blender’s model in .obj format into Rhino v7	29
Figure 9. Edmonton building footprints in QGIS v3.30 (Source: Edmonton - Open Data Portal, https://data.edmonton.ca/stories/s/City-of-Edmonton-Open-Data-Terms-of-Use/msh8-if28/ , Contains information licensed under the Open Government License – City of Edmonton)	30
Figure 10. Edmonton building footprints in .shp format in Rhino	31
Figure 11. Building simplification algorithm: (a) mesh scaling and alignment; (b) helper curve selection; (c) point collection designated for roof recreation; (d) point set considered for façade simplification; (e) building meshes; (f) bounding boxes for façade simplification; (g) projected 2D	

façade meshes; (h) projection of façade point set onto the 2D meshes; (i) outline rooftop curve; (j) simplified building geometry	34
Figure 12. Examples of the “Façade Segmentation” dataset: (a) Gunning/Lemieux Chemistry Centre at University of Alberta; (b) Google Street View of the Centennial Centre for Interdisciplinary Science (CCIS) building at University of Alberta (Image capture: Jul 2012 ©2023 Google); and (c) Sir Douglas Bader Towers in Edmonton.....	37
Figure 13. Horizontal (L_h) and vertical distance (L_v) of PV panels displayed in front view	44
Figure 14. PV array arrangement algorithm: (a) starting points and their associated first panels; (b) PV panel oriented based on specified β , γ , and r values, from top view; (c) location readjustment of PV panels in relation to the starting point (top view) (d) final PV layout.....	46
Figure 15. Snow coverage loss factors of PV generation for different tilt angles	48
Figure 16. Simplified geometry of CSC	56
Figure 17. Simplified geometry of NW-VVC	57
Figure 18. Training and validation loss during CNN model training	59
Figure 19. Training and validation IoU during CNN model training	59
Figure 20. Examples of the segmented façades with trained CNN: (a) University of Alberta Observatory; (b) West side of CSC; and (c) South side of CSC	61
Figure 21. A selection of rectified and filtered segmented masks: (a) CSC, west façade; (b) CSC, south façade	63
Figure 22. Projected final masks on the façades of the case study buildings: (a) CSC, south façade; (b) CSC, west façade; (c) CSC, east façade; (d) NW-VVC, south façade; (e) NW-VVC, west façade	65

Figure 23. (a) Optimum PV layout for the south façade of CSC building; (b) South façade of CSC building in Google’s 3D model (Imagery ©2023 Google, Imagery ©2023 CNES / Airbus, Maxar Technologies, Map data ©2023 Google).....	69
Figure 24. Optimum PV layout for the west façade of CSC building	72
Figure 25. (a) Optimum PV layout for the east façade of CSC building; (b) East façade of CSC building in Google’s 3D model (Imagery ©2023 Google, Imagery ©2023 CNES / Airbus, Maxar Technologies, Map data ©2023 Google).....	75
Figure 26. Optimum PV layout for the south façade of NW-VVC	77
Figure 27. Optimum PV layout for the west façade of NW-VVC.....	79
Figure 28. PV system configurations in different scenarios: (a) Scenario #1; (b) Scenario #2; (c) Scenarios #3, #4, & #5; (d) Scenarios #6 & #7	82

Chapter One: Introduction

Climate change presents a significant and pressing threat among the many challenges faced by humanity. In response, considerable international efforts have been made over the past few decades. These efforts encompass a range of activities, including extensive research endeavors and the establishment of numerous protocols and agreements aimed at mitigating greenhouse gas (GHG) emissions and reducing reliance on fossil fuels for energy generation. It is crucial to give special attention to the construction industry, as it is recognized as one of the most energy-intensive and environmentally damaging sectors. In fact, buildings alone account for approximately 40% of global energy consumption and GHG emissions [1], [2]. Over the past two decades, primary energy consumption and CO₂ emissions have witnessed significant increases, with growth rates of 49% and 43% respectively. On average, there has been an annual increase of 2% in primary energy consumption and 1.8% in CO₂ emissions from 1994 to 2014. The International Energy Agency (IEA) highlights that urban areas, which are home to half of the global population, are responsible for 73% of the world's total energy consumption and 70% of CO₂ emissions. Furthermore, the International Energy Outlook report projects a substantial 56% growth in global energy consumption from 2010 to 2040 [3]. In response to these trends, there has been a growing focus on sustainable construction practices and an increased adoption of renewable energy technologies (RETs) in the building sector. This shift is driven by the pressing need to reduce energy demand and mitigate environmental impacts [4].

Solar energy represents a plentiful and environmentally friendly source of power that can be harnessed through the use of Photovoltaic (PV) systems. PV technology has gained considerable recognition as a renewable energy solution, driven by its improving competitiveness and cost

parity with other technologies, as well as the growing awareness of its ability to effectively capture solar radiation on building surfaces, government initiatives, and increasing electricity demand. Figure 1 demonstrates that Canada, characterized by its vast landmass and diverse geographical features, holds significant potential for generating PV power. The availability of solar resources varies across the country, with southern regions like Edmonton and Calgary typically enjoying greater solar irradiance compared to their northern counterparts [5]–[7].

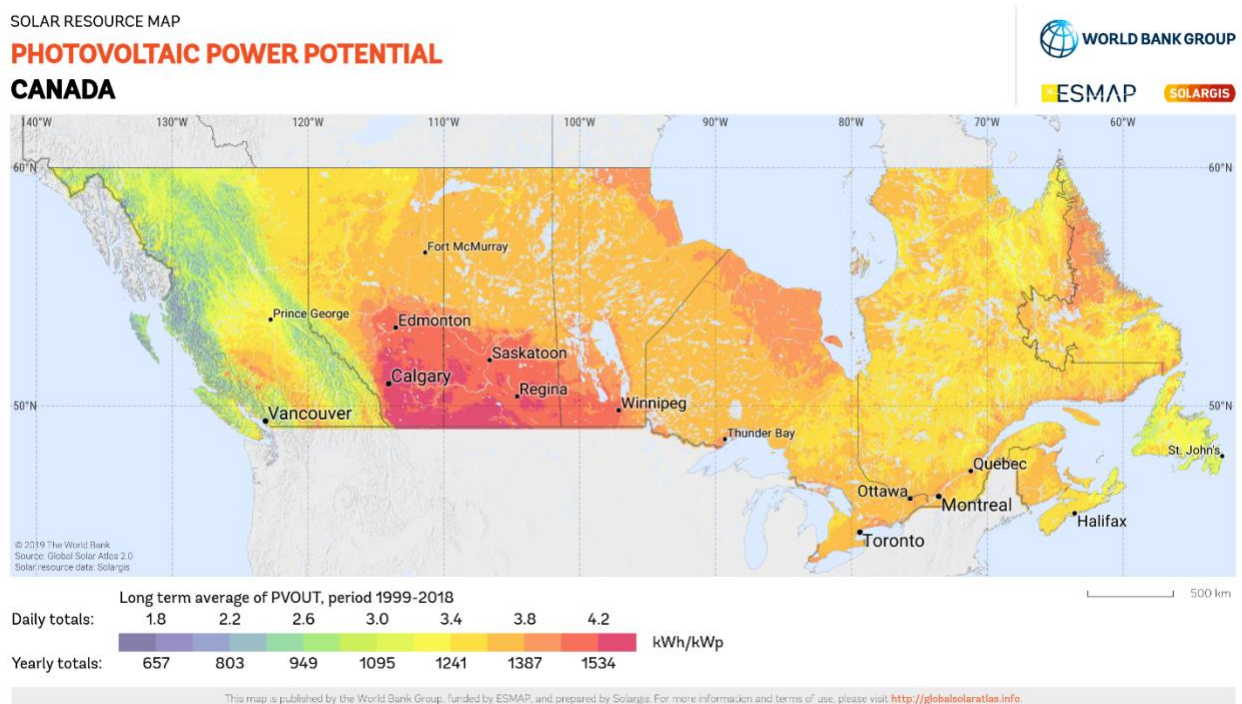


Figure 1. Photovoltaic electricity potential of Canada (Canada source: <https://solargis.com/maps-and-gis-data/download/canada>, © 2020 The World Bank, Source: Global Solar Atlas 2.0, Solar resource data: Solargis)

PV systems can be installed either on a building's rooftop or its façade to harness solar energy. Opting for façade installations offers certain advantages over rooftops. In tall buildings, unlike rooftops, the vertical surfaces of a building's façade are generally less shaded by vegetation, neighboring buildings, or other obstructions. This reduced shading enables better exposure to

sunlight, maximizing the potential for solar energy generation. Façades also tend to have more direct access to sunlight throughout the day, particularly on the sides of the building that receive ample sunlight [8]. Furthermore, façade-mounted PV systems provide enhanced opportunities for capturing solar radiation, particularly in high latitude regions where the sun's altitude angle is relatively low. The lower angle of the sun allows the vertical surfaces to receive sunlight more directly, increasing the efficiency of the PV system. Another advantage of utilizing the façade for PV installations is its impact on snow coverage. In regions with snowy winters, installing solar panels on the façade facilitates the sliding of snow off the PV modules, in contrast to rooftop installations. This reduces the accumulation of snow on the panels, ensuring better energy generation during winter months [9]. However, it is worth noting that snow-covered ground can actually enhance the reflection of solar radiation, leading to increased total incident solar radiation on PV panels and higher yields when the tilt angles are optimal. In fact, in locations such as snowy Switzerland, snow can increase local yield by up to 10% [10].

Considering these aspects, the façade of a building presents an attractive option for PV system installations due to the reduced shading in taller buildings, enhanced exposure to sunlight, and the advantage of snow management. However, it is important to conduct a thorough analysis of the specific building and its surroundings to determine the most suitable location for PV installations based on factors such as solar access, architectural constraints, aesthetic considerations, structural integrity, available space on the façade, and potential obstructions that may cast shadows on the panels.

1.1 Problem Statement & Research Objectives

The examination of various PV technologies for building façades is driven by the need to understand their impact on sustainability, including environmental, economic, and energy efficiency aspects. However, previous research has not adequately addressed these aspects collectively. Current efforts aim to develop an approach that enhances the optimization of PV installation parameters for façades. This approach involves automation in the classification of different façade elements and the consideration of shading effects caused by nearby objects, buildings, trees, etc., on electricity generation. The primary aim of this research is to establish a framework that empowers engineers and architects to make well-informed decisions regarding the selection of sustainable PV façade layouts for specific buildings. The comprehensive optimization framework considers the broader sustainability objectives, enabling practitioners to align their decisions with their specific project requirements and sustainability goals.

1.2 Thesis Structure

The current thesis comprises five main chapters, each focusing on specific aspects of the research topic. In this chapter, a concise introduction is provided, followed by a problem statement and the general objectives of the study.

Chapter two is dedicated to an extensive literature review, which aims to clarify the significance of the research objectives and underscore the need for such explorations. It begins by introducing different types of PV façade systems and then proceeds to review studies that have focused on PV façade optimization. Additionally, a review of studies exploring façade segmentation using deep learning approaches is presented. The chapter concludes by identifying the research gaps, defining the scope of the study, and highlighting its novelty.

Chapter three is divided into five main sections. Firstly, an overview of the tools and research workflow employed in the study is provided. The following section explains the developed methods for simplifying building geometry. Subsequently, the segmenting of façades, including the deep learning model developed and the segmentation dataset created, is discussed. The next section delves into the post-processing and perspective transformation techniques applied to the predicted segmented masks, along with their projection onto the corresponding surfaces in the 3D model. Lastly, the optimization framework, encompassing the design variables of the PV system and objective functions, is introduced.

Chapter four of the thesis presents the outcomes pertaining to building simplification, segmented façade masks, and the optimal arrangement of the PV system, with a specific focus on the economic and environmental factors. These results are showcased and discussed within the context of the case study buildings, and recommendations based on the outcomes are provided. Additionally, the solar radiation and energy simulation model utilized for the optimization phase are validated using available resources.

In conclusion, Chapter five of the thesis provides an overview of the contributions made and limitations encountered throughout the research. The chapter concludes by presenting valuable insights and recommendations for future research endeavors. It serves as a reflection on the findings and outcomes of the study, shedding light on the potential avenues for further exploration and development in the field.

Chapter Two: Literature Review

In this chapter, the different types of PV implementation for building façades are explained. Next, a comprehensive review is conducted on various studies dedicated to optimizing the PV layout settings for building façades, considering economic, environmental, or energy efficiency perspectives. The chapter also includes a review of different deep learning approaches utilized for façade parsing and segmentation. Finally, based on the results of the literature review, the research gaps are identified, and the significance of the present study is highlighted.

2.1 PV Façade Systems

PV modules offer the possibility of being installed on the external surfaces of buildings, leading to the concept of building applied PV (BAPV). BAPV involves retrofitting rooftops, façades, or other suitable areas of the building by attaching PV modules onto the existing building envelope using support structures or mounting systems. An alternative approach is the integration of PV directly into the building envelope itself, effectively transforming it into a functional architectural element or replacing traditional building materials. This integrated approach is known as building-integrated PV (BIPV). During the construction or renovation process, BIPV seamlessly incorporates PV modules into the structure of the building. A few examples of BAPV and BIPV applications are displayed in Figure 2. Both BAPVs and BIPVs play a vital role in driving the transition towards decarbonization and facilitating the development of more sustainable cities that embrace zero energy buildings. Their implementation aligns with the overarching goal of achieving energy efficiency and environmental sustainability in the built environment. [4], [11], [12].



(a)



(b)

Figure 2. Examples of BIPV & BAPV applications: (a) rooftop BAPV application (Image capture: May 2023 ©2023 Google); (b) semitransparent BIPV for facade application at University of Alberta

As mentioned earlier, there has been a growing global focus on promoting the adoption of PV in buildings, backed by policies and regulations that facilitate their seamless integration. In the literature, one can find various classifications that differ in their purpose, such as market analysis or research exploration, as well as criteria used, including technology, spatial relationship with the buildings, application types, and integration methods [11].

In the realm of optimizing design parameters for PV façade arrangements, the literature encompasses various types of PV façade applications. These applications can be broadly classified into the following categories, as mentioned in [13]:

1. Cladding Systems/Curtain Walls: This category involves the installation of PV modules as a cladding material on the external surface of the building façade, typically in the form of curtain wall systems. These curtain wall PV applications provide both energy generation and aesthetic enhancement, as the PV modules are seamlessly integrated into the building envelope, creating a visually appealing and functional façade.

2. Glazing Systems and Windows: PV modules are seamlessly integrated into windows, enabling them to generate electricity while allowing natural light to penetrate. Depending on the desired balance between transparency and energy generation, these PV windows can be transparent or semi-transparent.

3. External Accessories/Devices: This category includes PV modules integrated into shading devices such as louvers, awnings, sunshades, or balcony parapets. These shading devices not only provide protection from direct sunlight but also harness solar energy simultaneously.

4. Innovative Systems: This category encompasses unique PV façade systems such as double skin façades, moving or rotating parts of the façade, and active skins.

Each category of PV façade application offers distinct advantages and considerations in terms of energy generation, architectural design, and integration with the building envelope. The selection of the most suitable type depends on factors such as building orientation, aesthetic requirements, energy demands, and local climatic conditions. Considering the focus of the current work on adding PV panels to the wall parts of existing building façades, the application type would fall under Building Applied PV (BAPV) for cladding systems.

2.2 Optimizing PV Façade System Layout

Numerous research studies have focused on optimizing the arrangement of PV systems on building façades to enhance energy efficiency and minimize overall energy consumption by maximizing PV power generation. Some of these studies have particularly examined PV shading devices or PV glazing systems and considered the daylight performance of the PV system, including aspects such as visual comfort and glare mitigation. In their study, Jayathissa et al. [14] introduced a dynamic PV shading device (PVSD) and evaluated its performance using software simulations.

They conducted simulations for various dynamic configurations during each hour of sunlight and identified the most energy-efficient design. The results indicated that, depending on the efficiency of the mechanical heating and cooling system, implementing the dynamic PVSD could lead to energy savings ranging from 20% to 80% compared to a PV system with static panels. Abdullah and Alibaba [15] suggested the use of optimized responsive PVSDs with a dual axis tracking system as an efficient retrofitting method. They conducted energy performance simulations and also created a prototype of the responsive PV system to compare its performance with that of a traditional fixed application. The findings showed that the retrofit strategy could reduce energy consumption by approximately 33% compared to the existing building's performance. Sun et al. [16] conducted a comprehensive assessment of an office space that utilized semi-transparent photovoltaic (STPV) windows. Their study employed validated simulation tools including EnergyPlus, WINDOW, and RADIANCE to analyze the optical, electrical, and energy performance of the building. The researchers investigated different window designs across five distinct climates in China, focusing on the building's thermal properties, daylighting capabilities, and overall energy performance. The findings revealed that the implementation of PV windows resulted in superior performance compared to conventional double-glazing solutions. Liu et al. [17] conducted a comprehensive investigation into the impact of various factors, such as orientation, tilt angle, plot ratio, conversion efficiency, and geographic location, on the energy generation of BIPV systems. Their findings revealed that, for low-rise residential buildings in China, the southwest region of the country is the most suitable location for the development of zero energy buildings. Additionally, they highlighted the necessity of achieving a PV conversion efficiency higher than 20% for optimal energy generation. Building upon their previous research, Liu et al. [18] further examined the self-sufficiency and self-consumption aspects of PV systems

to identify the optimal design configuration for PV façades. The results indicated that, when the heating demand exceeds the cooling load, a higher tilt angle should be considered compared to the latitude of the specific location, whereas the opposite holds true when the cooling load surpasses the heating demand. Li et al. [19] introduced a novel PV system called PVPC façade, which involves integrating solar panels into a precast concrete (PC) façade. In this system, insulation and PV panels are positioned within a designated groove in the concrete wall, facilitating the installation process. The researchers conducted thermal and electrical performance simulations of the PVPC façade using real-time ambient temperature and solar radiation data. To validate the simulation results, a prototype of the PVPC façade was constructed. The findings revealed that the PVPC façade effectively generates electricity and reduces the building's energy demand, resulting in an annual energy savings of approximately 64.34 kWh/m². Cheng et al. [20] conducted parametric simulations to explore the performance of a double skin STPV window. The study investigated various design parameters including PV coverage ratios, window-wall ratios (WWR), and orientations to identify an optimized configuration. The findings indicated that the implementation of STPV windows improved the quality of daylighting within the building while also reducing energy consumption. By proposing the implementation of a PV double skin façade as a viable approach for enhancing building performance, Lee et al. [21] employed a combination of simulation tools and experiments to demonstrate the economic viability of this system in reducing energy demand. Taveres-Cachat et al. [22] integrated thermal, electric, and lighting simulations with multi-objective optimization techniques to parametrically optimize the design of PVSDs. The study showed that employing these methodologies can enhance solar harvesting and overall building performance. Chen, Yang, and Peng [23] introduced a design guideline aimed at optimizing the size, shape, geometry, thermal properties, and optical properties of windows in

early-stage design for high-rise commercial buildings situated in various urban contexts characterized by different densities. The study proposed two parameters, namely active glazing PV area and active wall PV area, to integrate PV modules into the building envelope. Through sensitivity analysis, the research demonstrated that the design of the PV envelope is influenced by window geometry and properties. In a separate study, Skandalos and Tywoniak [24] investigated the electrical, thermal, and daylight performance of four different configurations of PV façades. The researchers conducted dynamic thermal simulations to assess the effectiveness of these PV systems in reducing energy consumption and improving visual comfort. The studied PV layouts consisted of opaque vertical and tilted PV modules integrated into the building envelope as an alternative to conventional wall materials, STPV windows, and PVSDs. The findings demonstrated that the reference building incorporating inclined opaque PV modules exhibited the best energy performance, while the implementation of STPV windows resulted in optimal daylighting and visual comfort performance. Alrashidi et al. [25] conducted experimental measurements to evaluate the visible and solar transmission, as well as the solar heat gain coefficient (SHGC), of a semi-transparent PV window. By comparing these measurements with those of a single pane window, it was observed that the utilization of semi-transparent BIPV windows can effectively reduce energy consumption while generating additional electrical power. In another study aiming to identify the optimal BIPV window design in terms of overall energy performance and visual comfort, Mesloub, Albaqawy, and Kandar [26] investigated nine commercially available PV modules with different orientations, tilt angles, WWRs. Extensive simulations and experimental measurements were conducted, leading to the recommendation of a double-glazing PV window with a medium WWR as the optimal choice. This configuration could achieve up to 60% energy savings while mitigating glare issues compared to the reference building

prior to the implementation of PV technology. Mesloub et al. [27] investigated the potential advantages of utilizing PVSDs as a retrofit strategy for a prototype office. The study involved numerical simulations of various PVSD configurations, such as an inclined single PV panel, unfilled egg-crate PVSDs, two different PV systems with horizontal louvers, and an STPV system. The performance of each configuration was compared to assess their effectiveness in terms of reducing energy demand and minimizing glare. Experimental measurements were also carried out to determine the optimal tilt angle of 30° for the louvers. The findings demonstrated that the integration of PVSDs can lead to a significant decrease in energy demand and a reduction in glare within the office space. Florio et al. [28] introduced a comprehensive framework for estimating building energy consumption and the potential PV generation from visually appealing solar panels installed on walls. The framework utilized dynamic energy simulation tools such as Daysim, PVLIB toolbox in Python, MATLAB, and Rhino-Grasshopper 3D environment. In a conservative scenario, the study concluded that BIPV had the capability to fulfill 32% of the space heating energy demand in Geneva, Switzerland. Choi [29] introduced a unique PV façade concept to enhance the energy self-sufficiency of older buildings by maximizing the generation of solar power. The study presented a dynamic solar panel system that promotes energy independence and incorporates a kinetic façade design. This design allows the solar panels to adjust their tilt angle each month, optimizing the capture of solar energy. Feng et al. [30] developed a comprehensive framework based on mathematical modeling to evaluate the solar irradiation resources and potential for BIPV in different regions of China, considering the effects of partial shading. In order to validate the accuracy of their mathematical model, the researchers conducted simulations using both PVsyst software and the model proposed in their study to analyze the power generation of a PV array. The results demonstrated that rooftops are the most favorable locations for BIPV

installation, followed by south-facing façades, particularly in cities with higher latitudes. East and west façades also present viable options. Additionally, north-facing façades could be considered in certain cities characterized by frequent cloud cover.

Besides the studies mentioned earlier, certain research endeavors have integrated environmental considerations like GHG emissions or life-cycle assessment (LCA), into their investigations. In contrast, other studies have focused specifically on the economic aspects of PV façade installation, taking into account factors such as cost-effectiveness, or payback period (*PB*). Lu and Yang [31] conducted a study to assess the sustainability of BIPV systems by analyzing their energy payback time (*EPBT*) and greenhouse-gas payback time (*GPBT*) when installed on rooftops and façades. *EPBT* represents the duration it takes for a PV system to generate the same amount of energy that was expended in its production, while *GPBT* indicates the time needed for the PV system to offset the emissions created during its manufacturing and installation. The research findings highlighted the influence of installation orientation and location on the sustainability of the PV systems. Gholami and Nils Røstvik [32] conducted a life-cycle cost analysis (LCCA) to evaluate the economic feasibility of using BIPVs as a material for the entire building envelope. With a focus on the economic perspective, their study examined the potential of BIPVs to not only recover the initial investment cost but also generate income for the building. The findings indicated that this approach has the potential to be financially viable, offering a promising avenue for incorporating BIPVs into building designs. Vahdatikhaki, Salimzadeh, and Hammad [33] introduced a BIM-based generative design framework that utilizes multi-objective optimization for the layout design of PV modules on the entire exterior of tall buildings. The framework considers tilt and pan angles, as well as the presence of panels in specific locations (represented as binary variables), as design variables. The objectives of the optimization process are to minimize the cost and maximize the

revenue of the PV system. Through an extensive case study, the results demonstrated that the generative design framework can provide more favorable solutions, such as reduced costs and increased energy revenue, compared to baseline scenarios. It was observed that the majority of the studied scenarios favored optimal solutions that featured a consistent orientation of the panels, with consistent pan and tilt angles across all panels.

In the existing literature, some studies have explored the investigation of PV façade design characteristics with respect to more than one distinct dimension of sustainability, such as energy efficiency and economic factors. Sorgato, Schneider, and Rüter [34] conducted an analysis to evaluate the technical and economic feasibility of integrating frameless, glass-glass thin-film cadmium telluride (CdTe) PV modules on both the façade and rooftop of a commercial building. In terms of technical considerations, they determined that BIPV systems had the potential to fully meet the energy demand of the buildings. From an economic perspective, the replacement of conventional façade materials with PV modules was found to offer significant financial advantages. Economic assessment criteria, such as net present value, internal rate of return, and discounted payback time, were employed to evaluate the economic viability of the BIPV systems. Mendis et al. [35] undertook a study to determine the optimal design parameters for horizontally inclined PVSDs in a high-rise building, with a focus on energy performance and economic potential. The study considered design variables such as façade orientation, inclination angles, and distance-to-length ratio of panels in the PV system. Additionally, the economic potential of different shading strategies was evaluated, considering factors such as total cost and PB, to compare various installation methods. The results showed that the proposed optimal BIPV system can generate up to 8% more power compared to traditional vertical PV façade applications. Elghamry et al. [36] performed parametric simulations to analyze the effects of different variables

in a PV system on thermal and visual comfort, energy demand, PV generation, and CO₂ emissions. These variables encompassed the placement of PV cells on the façade (inside or outside the window), orientation, and location. The study employed a combination of numerical simulations and field measurements to evaluate these factors. The results demonstrated that integrating solar panels into the building façade can result in a significant 15% decrease in energy consumption compared to buildings without PV installations. This highlights the potential of PV façades in improving energy efficiency and reducing CO₂ emissions. Ansah, Chen, and Yang [37] combined a multi-objective optimization approach with building energy simulation and LCA to analyze the most suitable configuration of building envelopes in terms of their lifecycle performance. The study took into account several design variables, such as the WWR, orientation of PV systems (including BIPV windows and rooftop PV), façade infiltration rate, external wall material type, and external wall material thickness. The results of the optimized building design showed a remarkable reduction in lifecycle energy consumption, achieving up to 36.93% energy savings specifically in sub-Saharan Africa cities. Moreover, the implementation of PV systems allowed for efficient coverage of over 90% of the total energy demand of the building. Kurdi et al. [38] presented a novel framework for making design decisions, aiming to enhance the performance of PV systems at the neighborhood scale. The framework provides a unified interface for the development, evaluation, and interactive exploration of PV system designs, with the aim of achieving multiple design objectives. These objectives include increasing self-consumption (*SC*), reducing the *PB*, maintaining a higher level of self-sufficiency (*SS*) for the PV system, and minimizing the net load variance on the grid. The framework optimizes the orientation range of PV panels, considering tilt and azimuth angles, as well as the number of panels for each orientation. The results demonstrated that the optimized PV system, implemented in various scenarios,

emphasized a greater number of PV panels in south-west orientations. This design response was driven by the neighborhood's electricity demand patterns, particularly the higher demand and electricity prices in the evenings.

There have been limited research efforts focused on thoroughly investigating the potential influence of PV façade installations on sustainability indicators, including energy efficiency, environmental considerations, and economic factors. In their study, Liu et al. [39] conducted an independent analysis of various factors influencing the performance of BIPV in regions with high solar irradiance. These factors included PV module temperature, solar radiation intensity, PV module orientation and tilt angle, PV module types, and inverter efficiency. The feasibility of implementing BIPV systems in high solar-irradiance regions was assessed systematically, taking into account energy efficiency, environmental benefits, and economic performance. Energy efficiency and environmental benefits were evaluated using indicators such as greenhouse gas emission rate ($GHGE_{rate}$) and $EPBT$. The economic performance was assessed by analyzing the costs and benefits of PV systems. The findings indicated that the optimal installation position for PV modules on a façade is on the south-facing side at a tilt angle of 20° . In their study, Hadi and Heidari [40] compared three types of PV façades (CdTe, dye sensitized, and Perovskite) to determine the most sustainable option. They utilized energy analysis, LCA, and life cycle costing (LCC) methods to evaluate the economic and environmental aspects. Key indicators such as cumulative energy demand (CED), $GHGE_{rate}$, and $EPBT$ were considered for the life cycle analysis. The economic analysis included LCC and the levelized cost of electricity ($LCOE$). The results showed that the dye sensitized façade had the lowest cost, while the Perovskite façade was identified as the most sustainable option. The study also employed a hierarchical adaptive weighting (HAW) approach as a multi-criteria decision-making (MCDM) tool to combine criteria

from environmental, economic, and energy aspects into a sustainability index. The process of forming the HAW involved defining objectives, criteria, and options, followed by constructing a decision matrix and subsequently normalizing it. It was concluded that the choice of façade option may depend on the policy maker's perspective and approach, as suggested by the integrated LCC-LCA-HAW analysis.

2.3 Deep Learning for Façade Parsing

Many research studies have been dedicated to the task of façade parsing, which involves segmenting and labeling distinct elements such as windows, doors, balconies, and architectural details on a building's exterior. To tackle this task, advanced semantic segmentation models based on deep learning techniques have been developed. These models leverage the power of deep neural networks, particularly convolutional neural networks (CNNs), to accomplish the semantic segmentation task effectively. Semantic segmentation aims to assign a specific label to each pixel in an image, enabling the precise identification and classification of different objects or regions within the image. By employing this approach, researchers can conduct a comprehensive analysis and gain a deeper understanding of the various components present in a building's façade. Nishida, Bousseau, and Aliaga [41] developed an interactive tool for automatic procedural modeling grammar generation from a single building image. The process involves selecting a photograph and outlining the building silhouette. A pipeline employing CNNs, and optimization techniques creates building components, including mass, windows, and doors. Multiple stages are involved: estimating camera parameters and building mass shape, rectifying façades, recovering layout, and extracting windows and doors. Procedural grammars are selected for windows and doors in the final stage. The grammars are combined to generate a comprehensive procedural representation of the building. The method has been successfully applied to generate diverse procedural building

models from existing photographs. Liu et al. [42] presented a unique symmetric loss function that can be utilized in deep neural networks for comprehensive training. This innovative loss function takes advantage of the regular rectangular shape often found in windows and doors and penalizes non-rectangular window predictions. By seamlessly integrating this prior knowledge into the end-to-end training process, the model achieves superior performance compared to existing methods on five popular façade parsing datasets. Qualitative analysis demonstrates that the proposed approach enhances the accuracy, visual appeal, and symmetry of the predicted shapes produced by deep CNNs. Li et al. [43] presented a novel approach for window recognition in colored façade images using deep learning and heatmap fusion. Their model takes a color façade image as input and detects windows by identifying the key points, specifically the corners of windows. Unlike traditional methods that involve predicting bounding boxes or segmenting the entire façade, this approach focuses on localizing individual windows. To facilitate research in this field, the authors curated a dataset of 3418 annotated façade images. The proposed model achieved impressive performance, with a precision of 91.4% and a recall of 91.0% at an intersection over union (IoU) of 50% on their dataset, surpassing the performance of most other methods on publicly available test sets. Ma et al. [44] introduced a novel deep architecture for façade parsing that takes into account the challenges of occlusion and appearance ambiguity in single-view images. The key feature of this architecture is a cross-view feature aggregation module, which selectively incorporates relevant CNN features from nearby views to enhance the representation of the target view. By leveraging the advantages of the multiview enhanced representation, the proposed architecture effectively addressed the issues of ambiguity and occlusion. Comprehensive comparison experiments and ablation studies were conducted to showcase the strong performance of the proposed method, as well as the effectiveness and transferability of the cross-view feature

aggregation module. Liu, Li, and Zhu [45] proposed a novel approach that combines segmentation and anchor-free detection within a single-stage network, facilitating efficient training and improved convergence. Additionally, they introduced a novel refinement module based on translational symmetry to enhance the accuracy of the segmented maps. The researchers parsed the façades into shape grammars and utilized a rendering engine like Blender for the reconstruction of realistic high-quality 3D building models using procedural modeling techniques. The proposed approach was evaluated through quantitative and qualitative experiments on three widely used façade parsing datasets, and the results showcased the effectiveness of their translational symmetry-aware approach. Nordmark and Ayenew [46] investigated into the application of the Mask R-CNN framework for the detection of windows in façade images. Their study involved training the proposed model using transfer learning on pre-trained COCO weights, along with their own dataset of street view images of façades. The aim was to generate accurate instance segmentations specifically for windows. By leveraging transfer learning and employing data augmentation techniques, the experimental findings revealed that the proposed approach achieved performance comparable to that of existing state-of-the-art methods for window detection. Notably, their method achieved these results with a relatively small dataset, without the need for post-optimization techniques. In a separate investigation, Ma et al. [47] proposed the implementation of a pyramid atrous large kernel (ALK) network, known as ALKNet, for the semantic segmentation of façade images. The ALKNet utilizes ALK modules within multiscale feature maps to capture extensive dependencies among building elements. By harnessing the regular structures inherent in façades, the network effectively integrates nonlocal context information, enabling it to tackle challenging image regions characterized by occlusions and ambiguities. Experimental evaluations conducted on both rectified and unrectified façade datasets

demonstrated the superior performance of ALKNet compared to existing cutting-edge methods. Expanding upon their prior research, Ma et al. [48] presented a fresh approach to tackle the issue of occlusions in façade parsing through the utilization of progressive feature learning. In this study, they focused on identifying occluded regions by evaluating Bayesian uncertainty in pixel categorization. Leveraging this uncertainty information, they proposed an occlusion-immune façade parsing architecture that progressively refined pixel features in contaminated regions, starting from the easiest to the most challenging. Specifically, they prioritized refining the features of outside pixels, which benefit from reliable context from visible areas, at the early stages. To enhance the contextual information, they introduced a context enhancement module (CEM) that utilized directional strip kernels instead of regular square convolution kernels. These strip kernels effectively aggregated structural context to refine façade pixels. Extensive experiments conducted on widely used façade datasets demonstrated that the proposed method achieved excellent performance in façade parsing. In another research endeavor, Ma, Ma, and Xu [49] introduced a comprehensive deep network tailored for façade parsing in the presence of occlusions. The network is designed to adeptly decompose an input image into two distinct components: visible and invisible parts, achieved through occlusion reasoning. To enhance the semantic segmentation of the visible portion, the researchers proposed a context aggregation module that effectively gathers nonlocal cues. Additionally, acknowledging the inherent regularity of man-made structures, a repetitive pattern completion branch was devised to infer the content within the invisible regions by referencing the visible segment. Ultimately, by harmonizing the outcomes from the visible and invisible components, a parsing map for the input façade image is generated. Zhang, Pan, and Zhang [50] devised a hierarchical deep learning framework with a symmetric loss function to automatically detect building façade elements in images. The framework incorporates

spatial and channel attention modules to enhance performance. A novel loss function integrates prior knowledge to encourage well-proportioned shape detection of façade elements, including windows, doors, concrete walls, and sunshades. Experimental results on two public datasets demonstrated significant improvements over existing models. For example, on the Ecole Centrale Paris (ECP) dataset, the achieved IoU of 81.9% showed an improvement of 11.3% compared to the Fully Convolutional Network (FCN). On the ArtDeco dataset, the Mean IoU of 85.6% exhibited an improvement of 11.4% over FCN. The developed approach effectively detected regularized façade elements with high accuracy, achieving an IoU of 93.6% for wall components on the ECP dataset and 88.6% on the ArtDeco dataset.

2.4 Research Gap, Scope & Novelty

As more buildings embrace the shift from fossil-based energy sources to renewable energy, it becomes increasingly important to investigate the optimal PV layout that can maximize the contribution of PV systems to various sustainability aspects. This includes energy efficiency, economic considerations, and environmental impacts. However, there is limited research focusing on the comprehensive analysis of how PV façade design parameters impact these sustainability aspects. To the author's knowledge, there is a research gap in the development of a comprehensive framework that considers the impact of various design parameters of PV façade systems on energy efficiency, economic factors, and environmental sustainability. Previous studies have primarily focused on specific aspects rather than a holistic approach. Additionally, limited attention has been given to automatically extracting façades from 3D building models, classifying façade elements using deep learning, and identifying suitable areas for PV panel installation. Another limitation is the focus on providing guidelines for integrating BIPV systems in new construction projects, neglecting the importance of retrofit strategies for existing buildings. It is crucial to develop

practical frameworks that enable the selection of sustainable BAPV layouts for retrofitting purposes, making existing buildings more environmentally friendly and sustainable. The presented work offers substantial contributions that span both academia and industry. This multidimensional framework comprehensively addresses various facets of the field. From an academic standpoint, it advances the understanding of optimizing PV façade systems by incorporating considerations such as energy efficiency, economic feasibility, and environmental impact. On an industrial scale, this framework has the potential to enhance sustainable building practices. It provides a practical tool for architects, engineers, urban planners, and even municipalities to develop more energy-efficient, economically viable, and environmentally responsible PV façade systems. This empowers them to make informed decisions and contribute to the overall sustainability of the built environment. Consequently, the contributions encompass the advancement of knowledge within academia and the provision of a valuable tool for industry practitioners.

In light of the research gaps highlighted earlier, this thesis proposes a comprehensive workflow aimed at determining the optimal placement of PV systems on building façades, with a specific focus on commercial and educational buildings. The workflow encompasses the following key aspects:

- Optimizing the arrangement of PV panels on façades, considering the classification of façade elements, identifying installable PV areas, and accounting for shading effects caused by neighboring objects, buildings, trees, and other factors that may impact PV generation.
- Considering economic, environmental, and energy efficiency factors holistically in the decision-making process.

- Introducing optimal PV layout parameters for different orientations of façade parts, including south-facing, west-facing, and east-facing sections.

Chapter Three: Methodology

This chapter provides a comprehensive explanation of the developed methodology. It starts with a brief introduction to the tools used in the study. The chapter then proceeds to elaborate on the processes developed for the geometry extraction and mesh simplification of the three-dimensional (3D) building models. Afterward, it explains how different parts of the façades are segmented and classified using a deep learning model. The resulting predicted images undergo several image processing stages including perspective transformation, to enable projection onto the 3D models. Lastly, the chapter describes the multi-objective optimization process, which encompasses the design variables of PV system, solar radiation analysis, energy simulation model, and the objective functions.

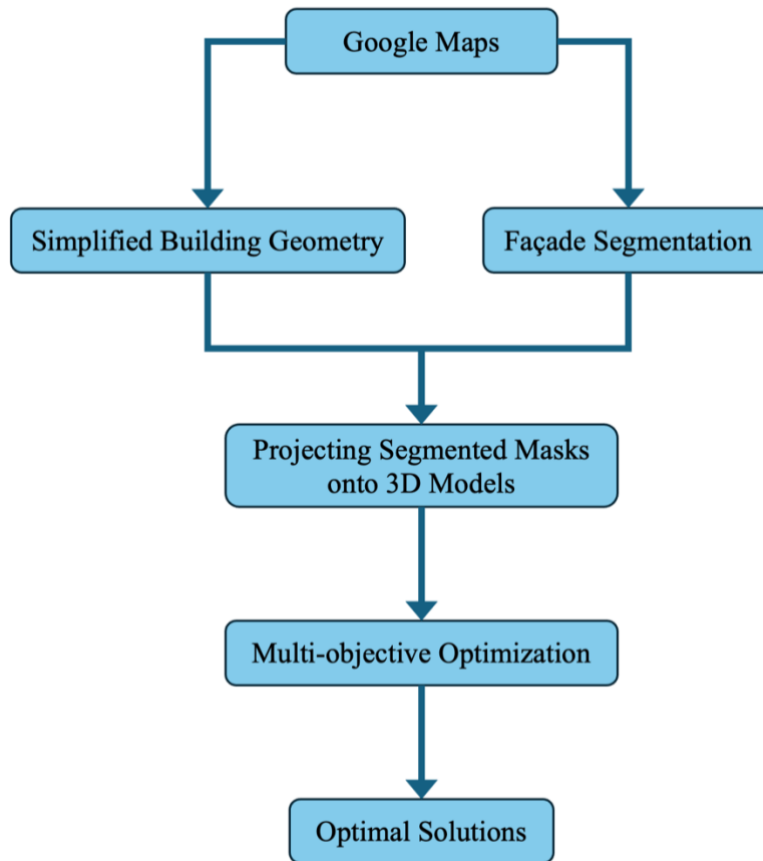
3.1 Overview

Figure 3a provides an overview of the developed framework's roadmap, while Figure 3b offers a more detailed visualization of the optimization framework, showcasing the specific procedures and tools utilized. The first step of the proposed approach involves recreating and simplifying the geometry of the target building using Google Maps 3D models and building footprints. Subsequently, the façade images are inputted into a deep learning model, enabling the identification of different components within each façade, such as the installable parts, which in this research are limited to walls, windows, and obstacles. The segmented masks resulting from the deep learning model undergo rectification or perspective transformation to align with the actual façades. Additionally, image processing techniques are applied, including the filtering of installable parts to create distinct black and white sections. The processed masks are then projected onto their respective vertical faces in the 3D model. In the final step, a multi-objective optimization

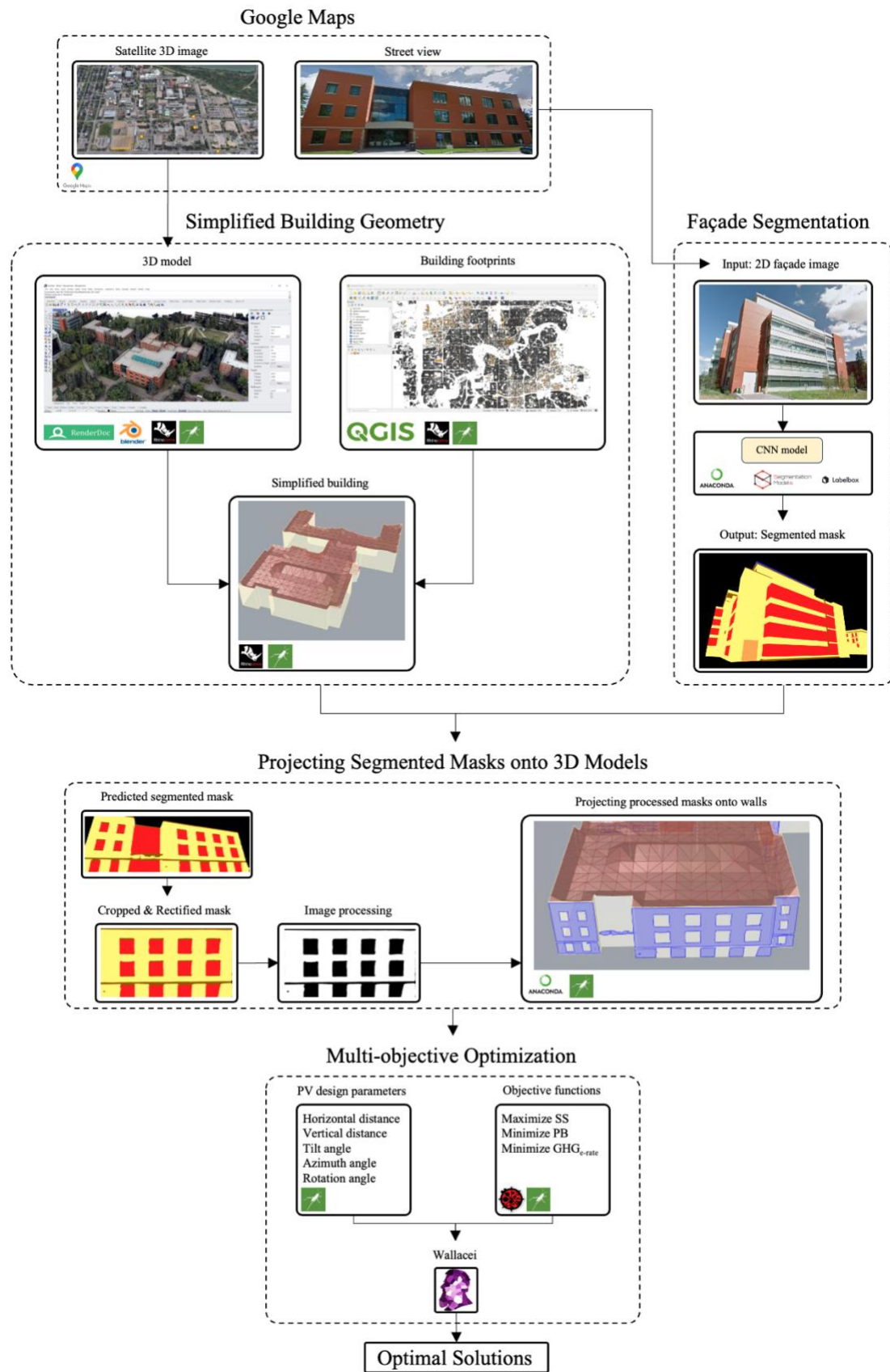
approach is employed to determine the optimal PV design variables. The optimization process takes into account the defined objectives, which prioritize energy efficiency, economic consideration, and environmental factors. The following sections provide a detailed explanation of each stage.

3.2 Simplified Building Geometry

First and foremost, it is essential to determine the geometry of targeted buildings in detail for projecting 2D filtered images, which classify different elements of each façade (such as walls, windows, doors, etc.), onto the envelope. Additionally, this allows for the placement of PV panels on the installable parts, which are defined as walls within the scope of this study.



(a)



(b)

Figure 3. (a) General overview of framework; (b) Detailed workflow of framework

3.2.1 3D Models of Buildings

The initial stage of extracting the buildings' geometry involves capturing the 3D models from Google Maps, which is achieved by utilizing the RenderDoc software. RenderDoc, an open-source graphics debugger, is the sole software capable of enabling frame capture for this purpose [51]. Figure 4 and Figure 5 showcase the Google 3D building models for the Computing Science Centre (CSC) and Northwest building of the Van Vliet Complex (NW-VVC), respectively. These buildings, which are located in the North campus of the University of Alberta, serve as the case studies within this research. Figure 6 presents a screenshot of the University of Alberta's buildings captured using the RenderDoc program in .rdc format. Next, the captured 3D models are imported into Blender, an open-source 3D computer graphics software tool set [52], by utilizing the "Maps Models Importer" add-on [53]. Finally, the format of 3D models is adjusted to .obj to enable the import of their meshes into Rhinoceros 3D, a computer graphics and computer-aided design application software [54]. Figure 7 displays the Google 3D model imported into the Blender software, while Figure 8 depicts the same model imported into the Rhino software. Notably, Blender was chosen for its remarkable versatility, open-source nature, and compatibility, offering an efficient and effective solution for the essential conversion of rdc files in the research, with limited alternative options available. Furthermore, the selection of Rhino was driven by its compatibility with vital plugins such as Ladybug Tools, which play a pivotal role in ensuring precise energy and daylight simulations and proficient image mapping onto 3D models, enhancing the research's overall quality and comprehensiveness.



Figure 4. Google's 3D model of CSC (Imagery ©2023 Google, Imagery ©2023 CNES / Airbus, Maxar Technologies, Map data ©2023 Google)



Figure 5. Google's 3D model of NW-VVC (Imagery ©2023 Google, Imagery ©2023 CNES / Airbus, Maxar Technologies, Map data ©2023 Google)

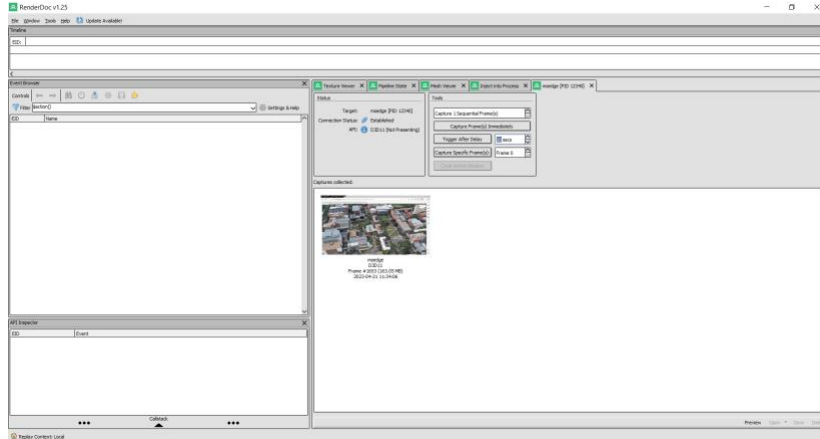


Figure 6. Captured Google's 3D model in .rdc format using RenderDoc v1.25

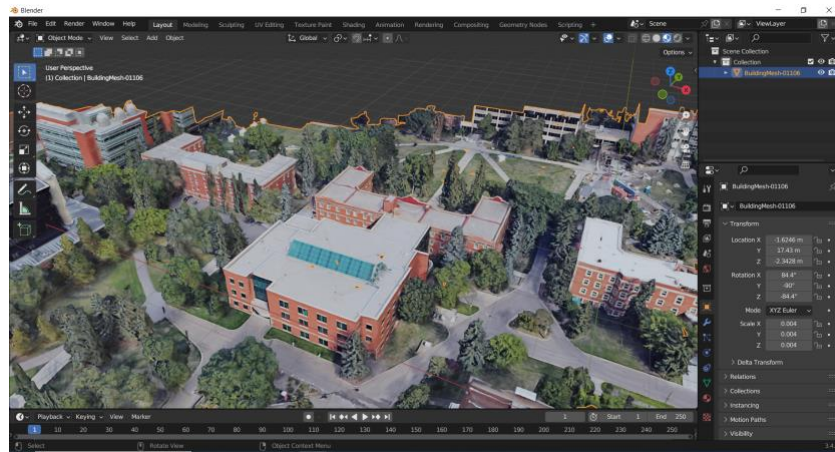


Figure 7. Imported Google Maps Capture into Blender v3.4.1

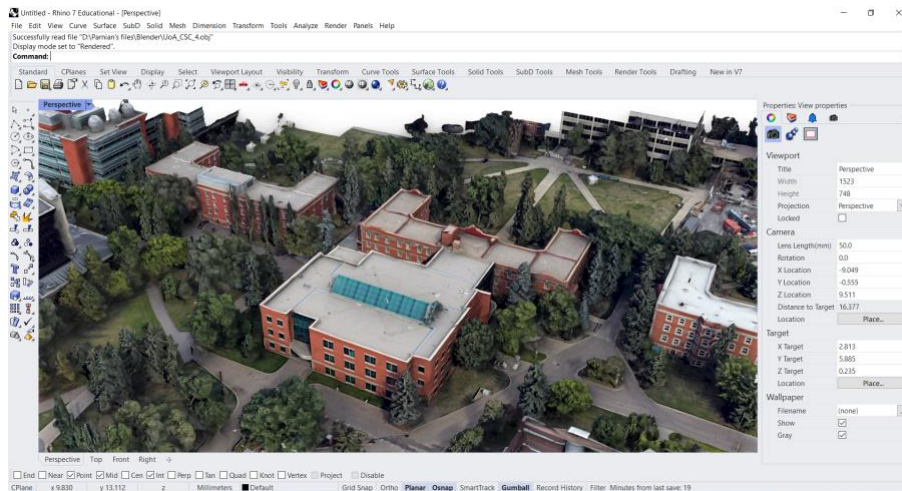


Figure 8. Imported Blender's model in .obj format into Rhino v7

3.2.2 Building Footprints

The algorithms developed for mesh simplification and building geometry definition primarily rely on the footprints of the buildings. Given that the case studies are situated at the University of Alberta, the building footprints of Edmonton are obtained by importing data from the City of Edmonton's Open Data Portal website [55], [56]. As showcased in Figure 9, the downloaded data files are then opened with the QGIS software which is an open-source cross-platform desktop geographic information system application [57]. Once the coordinate reference systems of the footprints are adjusted to "NAD83/ Alberta 3TM ref merid 114 W" (with the Authority ID of EPSG:3776), they are imported into Rhino in .shp format. This is achieved by utilizing the Grasshopper plugin, a visual algorithm editor for Rhino that employs a graphical programming language [58], [59]. A specific component called "Import SHP" is employed for this purpose (Figure 10).

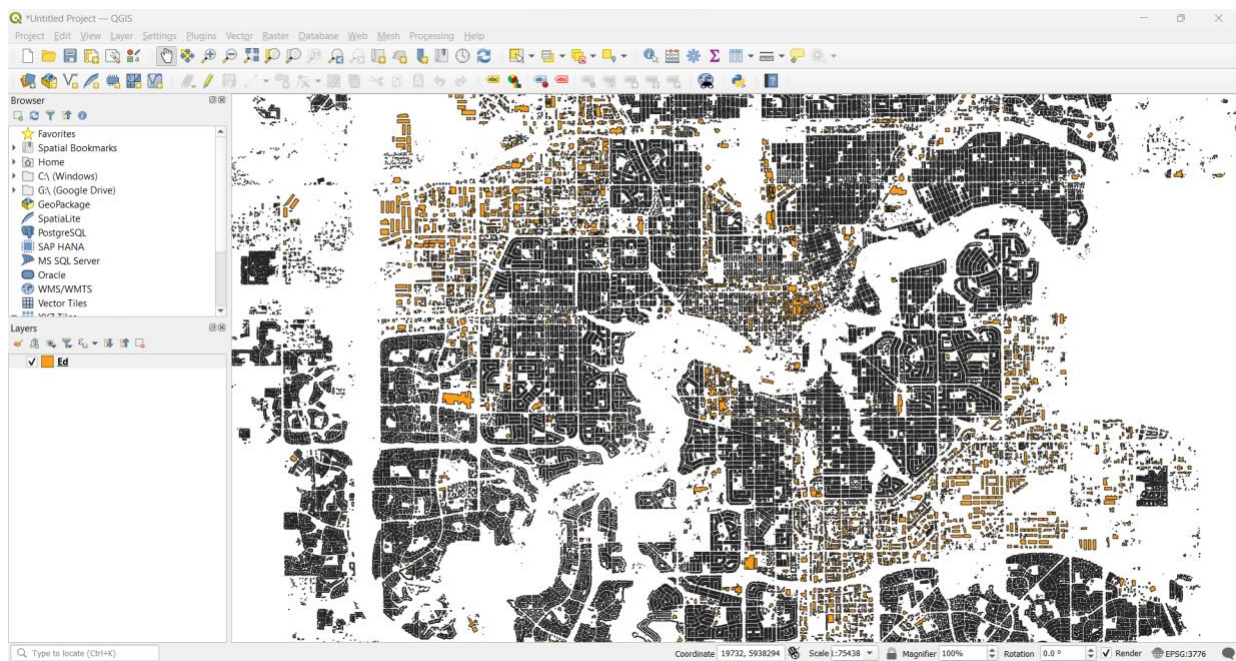


Figure 9. Edmonton building footprints in QGIS v3.30 (Source: Edmonton - Open Data Portal, <https://data.edmonton.ca/stories/s/City-of-Edmonton-Open-Data-Terms-of-Use/msh8-if28/>, Contains information licensed under the Open Government License – City of Edmonton)

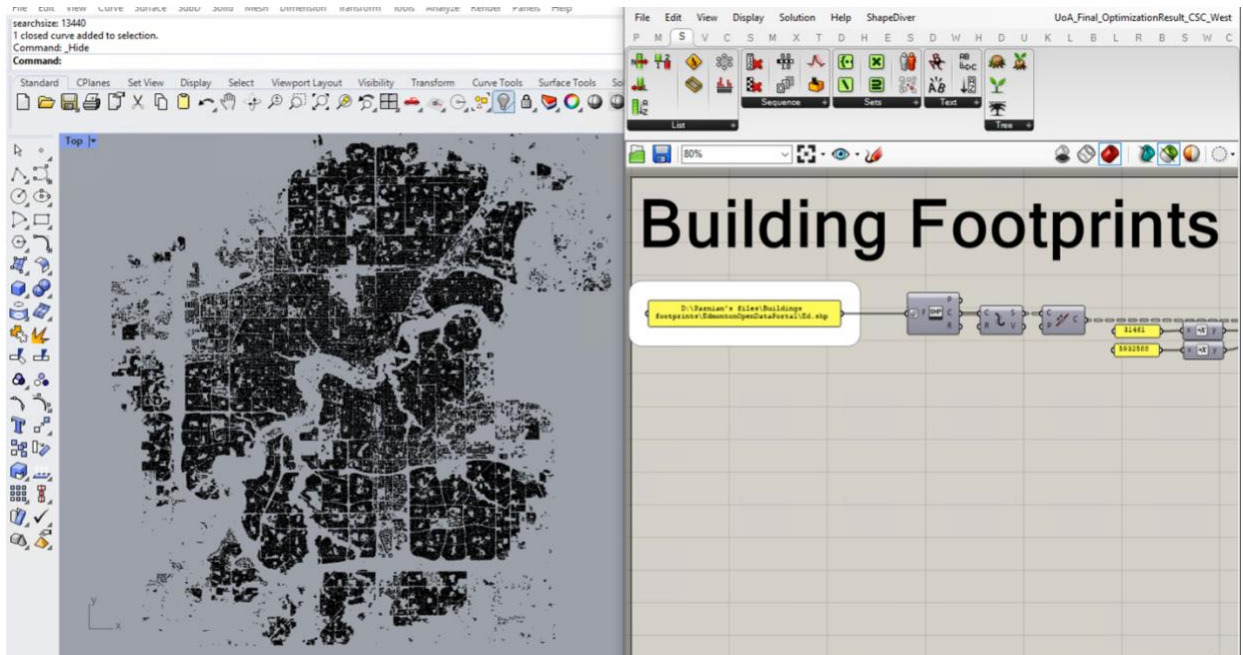


Figure 10. Edmonton building footprints in .shp format in Rhino

3.2.3 Simplification & Recreation of Building Meshes

After the scaling of the imported meshes from Blender, as discussed in section "3D Models of Buildings" and aligning them with the footprints (Figure 11a), the next step involves the user selecting a helper curve that encloses the footprint of the desired building (Figure 11b). This selection initiates the simplification algorithm, which then focuses its operations on the specified building. To enhance the computational efficiency of the model, the initial step involves reducing the number of imported meshes by 50%, as depicted in Figure 11a. Subsequently, a set of equidistant points, spaced at 3 meters, is chosen within the building footprint area. It is worth noting that the distance between these points can be adjusted, with the option of decreasing it to achieve higher accuracy in the output simplified geometry. However, such a modification would also increase the computational intensity in this scenario. As the focus of this research is on PV installation on building façades, all intersection points found on the line segments of the building footprint are also included in the point collection. This inclusion aims to enhance the accuracy of

the building façades during the simplification process. For the purpose of simplifying both the façades and the roof, two distinct sets of points are taken into account. The point set considered for creating the simplified roof geometry encompasses all points positioned either inside or on the building footprint. On the other hand, the point collection designated for generating simplified façades solely comprises the points located on the building footprint (Figure 11c, and Figure 11d).

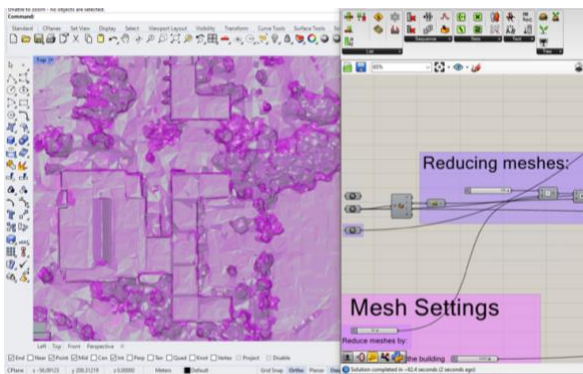
3.2.3.1 Façade Simplification

To isolate the meshes for each vertical face of the building envelope, imaginary bounding boxes are created. These bounding boxes are generated based on the building footprint, where the footprint is extruded to create surfaces that encompass the lowest and highest points of the vertices of the building meshes within the footprint area. The building meshes are showcased in Figure 11e. Subsequently, the generated surfaces are offset by 1.1m outward and 0.6m inward to construct the bounding boxes (Figure 11f). Afterwards, the 3D meshes encompassed within these bounding boxes are projected onto the imaginary vertical surfaces that intersect the building footprint, resulting in their conversion into 2D meshes (Figure 11g). The point set mentioned earlier, intended for façades recreation, is elevated above the entire building meshes. It is then projected downward onto the generated 2D meshes. As displayed in Figure 11h, the elevated points are indicated by red dots, while the green dots represent the projected points. The resulting points are connected to form a closed curve, representing the outline of the rooftop (Figure 11i). Following this, the outline curve is extruded in the direction perpendicular to the façades, creating a surface used for cutting aforementioned imaginary vertical surfaces. The lower portion of the surfaces represents the façades of the building.

3.2.3.2 Roof Recreation

In this stage, the process follows a similar approach to the previous section. By lifting the points within the collection assigned for roof simplification, positioned inside the footprint but not directly on it, above the entire building geometry, these points are projected downwards onto the roof meshes. The resulting points are then combined with the projected points that shape the outline curve of the rooftop. The merged points are then utilized to construct a mesh, representing the roof of the building, as depicted in Figure 11j.

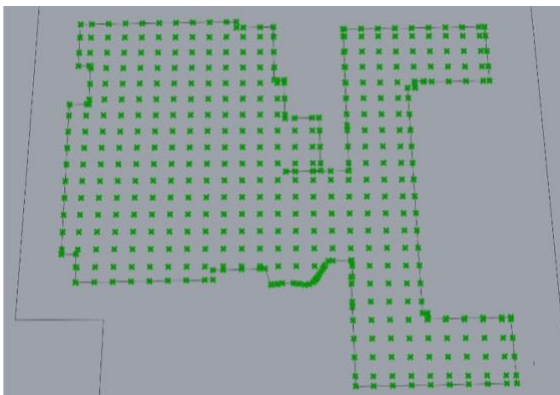
By juxtaposing the surfaces generated from the "Façade Simplification" and "Roof Recreation" sections with the boundary surface derived from the footprint, a closed and simplified volume of the building is formed. This volume serves a dual purpose as it is not only utilized for the PV placement and generation analysis but also enables energy model simulation.



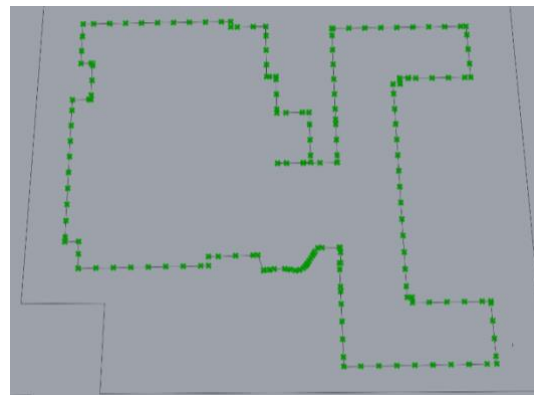
(a)



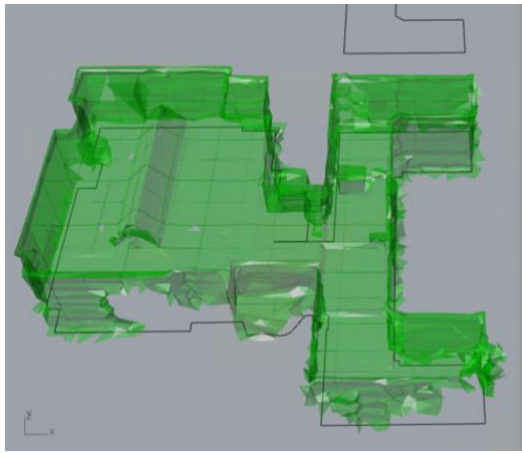
(b)



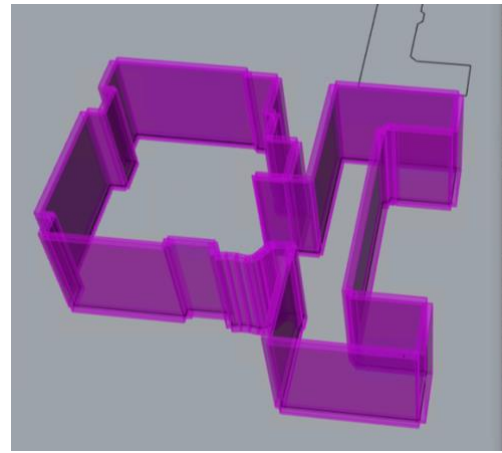
(c)



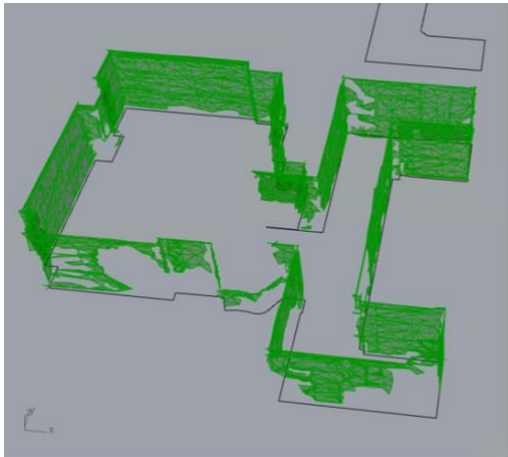
(d)



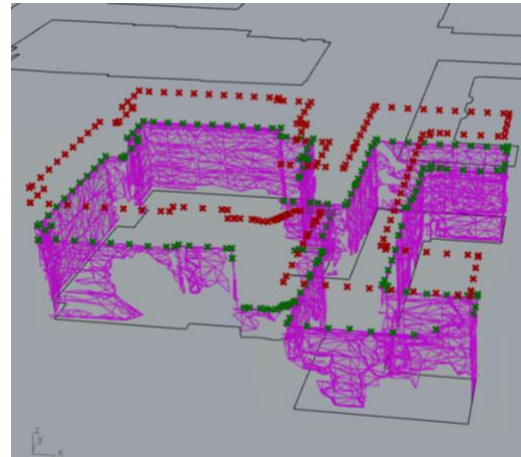
(e)



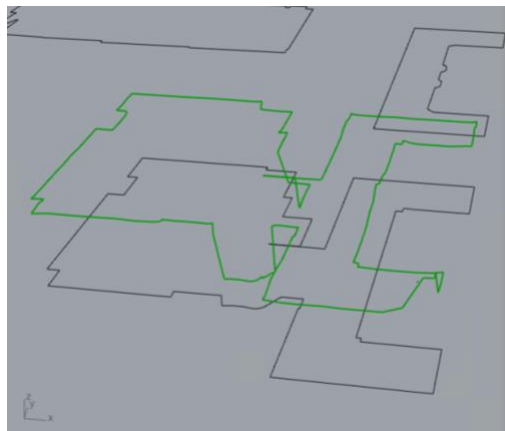
(f)



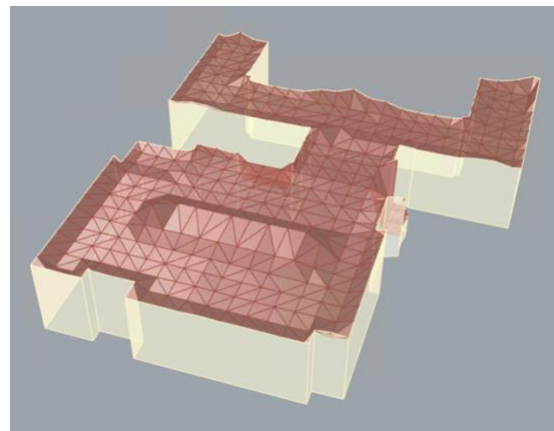
(g)



(h)



(i)



(j)

Figure 11. Building simplification algorithm: (a) mesh scaling and alignment; (b) helper curve selection; (c) point collection designated for roof recreation; (d) point set considered for façade simplification; (e) building meshes; (f) bounding boxes for façade simplification; (g) projected 2D façade meshes; (h) projection of façade point set onto the 2D meshes; (i) outline rooftop curve; (j) simplified building geometry

3.3 Façade Segmentation

This section provides a detailed explanation of the approach employed for wall identification within various façade elements. It covers the dataset that was used for training the model, the developed deep learning model, and the process of segmenting the images.

3.3.1 Façade Segmentation Dataset

The currently available façade datasets, such as eTRIMS [60] and ParisArt-Deco [61], primarily focus on European buildings which have architectural styles different from those found in the buildings of Edmonton. On the other hand, datasets like CMP [62] that include a wider range of architectural styles and cities, contain rectified images that are captured from a front-parallel perspective. Relying solely on datasets with rectified images for training hampers the ability to accurately segment façades in real-life scenes without perspective transformation. To address this limitation, a new dataset named the "Façade Segmentation" dataset has been created and annotated using the Labelbox platform [63]. The data was collected from four different sources, including photographs taken by the author using a personal phone camera from buildings in Edmonton and the University of Alberta, images from Google Street View and the internet, as well as some images from the window instance segmentation dataset [64], [65]. Table 1 displays the distribution of images obtained from each data source and provides the overall count of images and

Table 2 presents the seven object classes annotated in the database, along with their associated color labels and RGB channel values. A few examples of captured photographs and their corresponding segmented masks are illustrated in Figure 12.

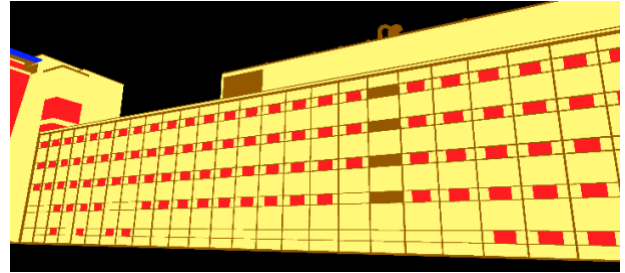
The dataset is randomly partitioned into three sets: the training set, which comprises 60% of the total images; the validation set, which accounts for 20% of the total images; and the test set, which also represents 20% of the total images.

Table 1. Details of "Façade Segmentation" dataset

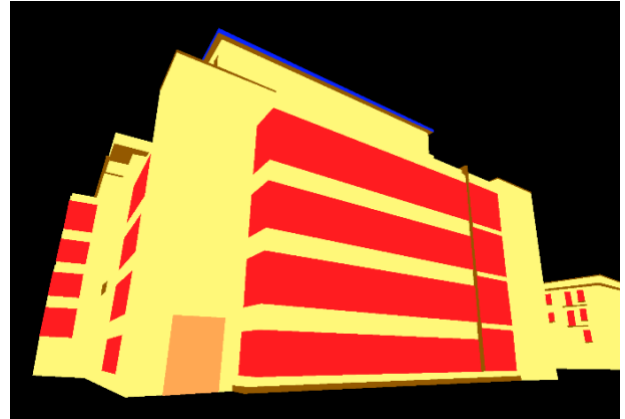
Image source	Count
Photographs captured by the author:	
University of Alberta	120
City of Edmonton	30
Google Street View	60
Internet	30
Existing dataset (window instance segmentation dataset)	22
Total	262

Table 2. Class names and their corresponding label colors

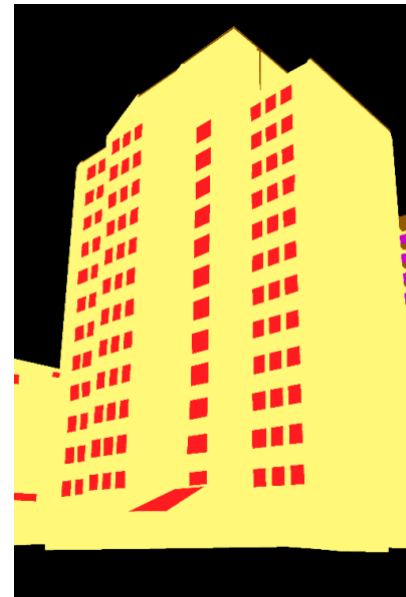
Class name	Label color	RGB channel values
Wall	Yellow	(255, 248, 121)
Window	Red	(255, 28, 32)
Door	Orange	(255, 168, 83)
Obstacle	Brown	(148, 89, 0)
Roof	Blue	(9, 36, 255)
Balcony	Purple	(206, 2, 206)
Background	Black	(0, 0, 0)



(a)



(b)



(c)

Figure 12. Examples of the “Façade Segmentation” dataset: (a) Gunning/Lemieux Chemistry Centre at University of Alberta; (b) Google Street View of the Centennial Centre for Interdisciplinary Science (CCIS) building at University of Alberta (Image capture: Jul 2012 ©2023 Google); and (c) Sir Douglas Bader Towers in Edmonton

3.3.2 Deep Learning Model Development

This study employs DeepLabv3+, a cutting-edge CNN architecture specifically designed for semantic image segmentation tasks. DeepLabv3+ is an extension of the DeepLab model series, originally created by Google Research. The "+" in DeepLabv3+ signifies the inclusion of an encoder-decoder structure, which integrates spatial information from various scales. This architectural enhancement enables the model to capture both local and global context, resulting in improved delineation of object boundaries and effective handling of objects at different sizes [66].

3.3.2.1 Model Setup and Configuration

To establish the pixelwise segmentation model based on DeepLabv3+, the setup includes the installation of Anaconda. Anaconda is a popular open-source distribution of Python and R programming languages for data science and machine learning tasks [67]. Anaconda includes Jupyter Notebook, a web-based interactive computing environment, which is utilized for developing all the façade parsing related parts of the research [68]. The implementation involves leveraging various software packages and Python libraries, specifically Python 3.10.9, PyTorch 2.0.1, OpenCV 4.7.0.72, Albumentations 1.3.0, (a Python library for image augmentation) [69], [70], and an essential component called Segmentation Models PyTorch (SMP) 0.3.3. SMP is a Python library built on PyTorch, offering neural network-based image segmentation capabilities [71]. Furthermore, Patchify 0.2.3 is utilized to split images into small overlapping patches based on a specified patch cell size, enabling subsequent merging of these patches back into the original image [72].

Regarding the configuration of the CNN model, the encoder is specified as ResNet-50, initialized with weights pretrained on the ImageNet dataset. This initialization aids in faster and more effective convergence during training. Given that the model is trained for multiclass segmentation,

the activation function chosen is Softmax. The training process utilizes the Adam optimizer, with an initial learning rate of 5×10^{-5} and a weight decay of 10^{-4} that undergoes tuning over 70 epochs. The weight decay is applied to improve the model's generalization performance and prevent overfitting. The dice loss is employed as the selected loss function, while the IoU score is utilized for evaluating the model's performance.

3.3.2.2 Training Set Preparation

Considering the limited memory of the graphics processing unit (GPU), the CNN model is trained using smaller-sized images and their corresponding labels. To achieve this, each image is initially cropped to ensure its height and width are divisible by the selected patch size, which in this research is set to 512. Consequently, each image is divided into non-overlapping smaller images with dimensions of 512×512 pixels. This partitioning is accomplished using the Patchify library mentioned earlier.

To expand the training data, augmentation techniques are applied using the Albumentations library mentioned previously. These augmentation processes encompass various operations such as random horizontal or vertical flipping, random 90° rotations, and random channel-wise shifts for the RGB input image. Furthermore, each image undergoes preprocessing transformations, including data normalization, which may vary based on the specific pretrained neural network utilized. Additionally, due to GPU memory limitations, a batch size of 16 is employed for the training set, while a batch size of 8 is used for the validation set.

3.4 Combining 2D Images with 3D Models

Following the training of the CNN model, perspective transformation or rectification techniques are implemented on the segmented masks to achieve precise alignment and maintain visual

consistency. These techniques adjust the perspective of the masks, aligning them with the geometry and orientation of the corresponding vertical faces in the 3D building model. Additionally, the rectified segmented masks, representing the identified façade elements, undergo additional image processing to isolate the PV installable parts. In this study, the PV installable parts specifically refer to the walls. This isolation step is carried out to prepare the masks for projection onto their respective vertical faces within the 3D model.

3.4.1 Rectification & Image Processing of Predicted Segmentation Masks

The images obtained from the vertical faces of the desired building are subjected to several processing steps before being fed into the trained CNN model. Similar to the process described in the "Training Set Preparation" section, these images are initially divided into smaller patches and undergo preprocessing to prepare them for input into the model. Once the model generates a pixelwise segmented mask for each patch, the patches are reassembled to reconstruct the complete, predicted mask for the original image. Next, the user has the option to select the corners of a polygon-shaped area within the original image. This allows for cropping and retention of only the selected area, facilitating focused analysis. In the subsequent image rectification step, the perspective warping function in OpenCV is employed. The user is required to select the four corners of the vertical face of the building in a clockwise order (top-left, top-right, bottom-right, bottom-left). By utilizing approximate measurements of the building's height and width from the Google Earth application [73], a transformation matrix is calculated. This matrix is then used to apply a perspective transformation to the entire input image within the closed area defined by connecting the four selected corners. Simultaneously, all these processes will be automatically applied to the corresponding predicted mask of the given image.

After the rectification of the predicted mask, further processing is performed to enhance its suitability for the PV installation algorithm. The aim is to simplify the representation of the mask by converting it into a black and white format. To achieve this, the installable parts, which in this case are the walls, are designated with the color white. This means that the pixels corresponding to the walls in the mask are set to white. On the other hand, all other class labels present in the mask, such as windows, doors, or other façade elements, are converted to black. This conversion entails changing the color of the pixels representing these elements to black. By transforming the predicted mask in this manner, it becomes easier for the PV installation algorithm to identify and work with the walls as distinct entities. The clear differentiation between the white-colored walls and the black-colored non-installable elements simplifies the subsequent steps of the algorithm, allowing for more accurate and efficient PV installation planning.

3.4.2 Projecting Processed Masks onto 3D Models

During this stage, the filtered black and white masks are projected onto their corresponding vertical faces in the 3D model. If a mask includes multiple vertical faces, they are cropped and processed separately within the projection algorithm. The projection algorithm takes the filtered mask for each façade segment and its corresponding line segment in the building footprint as inputs. The white parts of the mask are converted into meshes using the Shapediver plugin for Grasshopper [74]. To simplify the complexity of the meshes, mesh reduction techniques are applied, and then the meshes are joined together. Using the "Rectangle Mapping" component in Grasshopper, the resulting meshes are projected onto the vertical surfaces along the selected line segment of the footprint. This projection process is repeated for all vertical faces of the targeted building. By following this procedure, the filtered masks are accurately mapped onto their respective vertical surfaces in the 3D model, ensuring the proper representation of the façade elements.

3.5 Optimization Framework

In this section, the details of PV system optimization are covered, including the design variables of the PV array, the algorithm for hourly power generation considering the shading effects of surrounding objects and mutual shading of the panels, the hourly energy demand of the targeted building, and the four objective functions considered in this study.

3.5.1 PV System Design Parameters

Generally, the PV placement algorithm involves five primary design parameters for configuring the layout of the panels. These parameters include the horizontal and vertical distances between the panels, the tilt angle of the panels, the azimuth angle of the panels, and the rotation angle of each panel within the layout. The concept of horizontal and vertical distance is illustrated in Figure 13. When we project the panels onto a horizontal plane, the distance between each pair of adjacent lines formed by the projection (shown in blue) represents the horizontal distance of the panels (L_h). Similarly, the vertical distance (L_v) refers to the distance between two adjacent lines formed by the projection of the panels onto a vertical plane (displayed in orange). To ensure computational efficiency, a minimum distance of 0.5 meters is enforced between panels when the lengths of the blue and orange lines are below 0.5 meters. This prevents the panels from being placed excessively close to each other, ensuring logical spacing. The azimuth angle (γ) of the PV module is defined as the angle between the projection of the module's normal on the horizontal surface and the local meridian plane. It ranges from -180° to 180° , where zero represents the south orientation, negative values indicate eastward orientation, and positive values indicate westward orientation. The tilt angle (β) of the PV module is the angle between the module and the horizontal surface. It varies from 0° to 180° , representing the inclination of the module with respect to the ground [75]. Additionally, the rotation angle (r) determines the panel's rotation around its normal axis, ranging

from 0° to 180° . An angle of 0° indicates a panel in landscape orientation, whereas an angle of 90° signifies a panel in portrait orientation, with rotation occurring clockwise.

With regard to the allowable range for the horizontal and vertical distance, the upper limit is estimated based on the longest shadow length of the PV panels. For the vertical distance, this length occurs during the summer solstice around noon, while for the horizontal distance it is calculated around noon when the sun's radiation is at its highest values. It is important to mention that in the northern hemisphere, the sun rises from the east and sets in the west. As a result, the north-facing faces of the building receive little to no direct sunlight throughout most of the year. This is why the azimuth angle is limited to a range of -90° to 90° . Additionally, the tilt angle can vary between 0° and 90° as it is not logical to orient the panels towards the building faces. In summary, the design variables of the PV system, their allowable ranges and intervals are defined as follows:

$$\begin{aligned} 0.0 \text{ m} < L_h < 2.5 \text{ m} & \text{ (intervals of 0.5m);} \\ 0.0 \text{ m} < L_v < 3.5 \text{ m} & \text{ (intervals of 0.5m);} \\ 0^\circ \leq \beta \leq 90^\circ & \text{ (intervals of } 10^\circ\text{);} \\ -90^\circ \leq \gamma \leq 90^\circ, & \text{ intervals of } 30^\circ\text{;} \\ 0^\circ < r < 135^\circ & \text{ (intervals of } 45^\circ\text{)} \end{aligned} \tag{1}$$

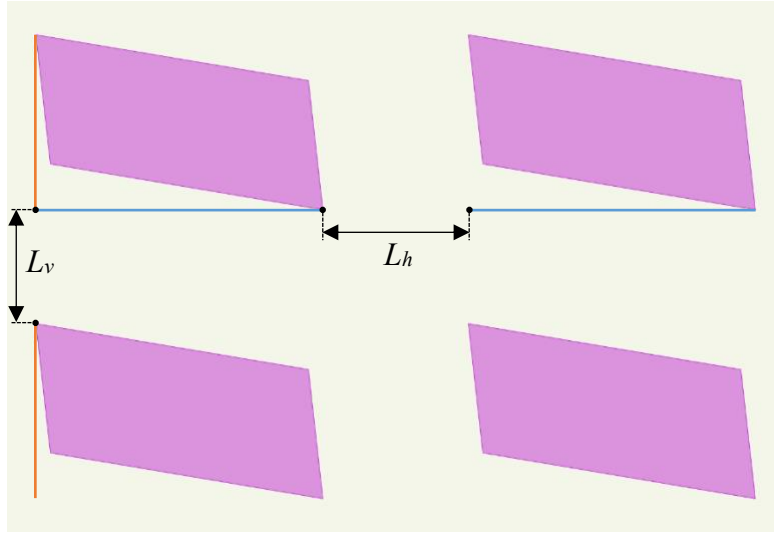


Figure 13. Horizontal (L_h) and vertical distance (L_v) of PV panels displayed in front view

The PV module used in this study is a product manufactured by CanadianSolar, and Table 3 provides an overview of its key features [76], [77].

Table 3. PV module specifications

Property	Value
Module name	CS3W
Cell type	Poly-crystalline
Maximum nominal power	420 W
Module efficiency	19.0%
Length	2108 mm
Width	1048 mm

In the PV arrangement algorithm, the placement of PV panels starts with selecting a starting point for each vertical face, initially set as the top left corner of the face. However, it was observed that due to variations in the upper edge of the recreated façades, some points may be lower than the starting point, causing a portion of the upper panels to extend beyond the face and be removed from the PV array. To address this, the height of the starting point is adjusted to be slightly lower

than the height of the original top left corner, considering the average height of the upper edge points that are up to 0.5m below the top left corner vertex.

The starting points also serve as the top left corner of the first panel for each building face. In Figure 14a, the starting points and their corresponding panels for the west-facing walls of the CSC building are illustrated. The panels are then positioned based on the specified azimuth and tilt angles. It is worth noting that in the initial placement, the panels may be located within the building's footprint. Therefore, the positions of the first panels are further adjusted relative to the starting points to ensure they are positioned correctly within the vertical face, neither inside nor outside the building footprint. An illustration of the location readjustment process can be seen in Figure 14b and Figure 14c from the top view. Following this, the initial PV panels are distributed across the vertical faces using the provided horizontal and vertical distances for the PV system. Only the panels that have their projected geometry within the projected mesh area representing the wall parts of the façade are included in the final PV layout (Figure 14d). These selected panels are then utilized in the next stage of the optimization framework.

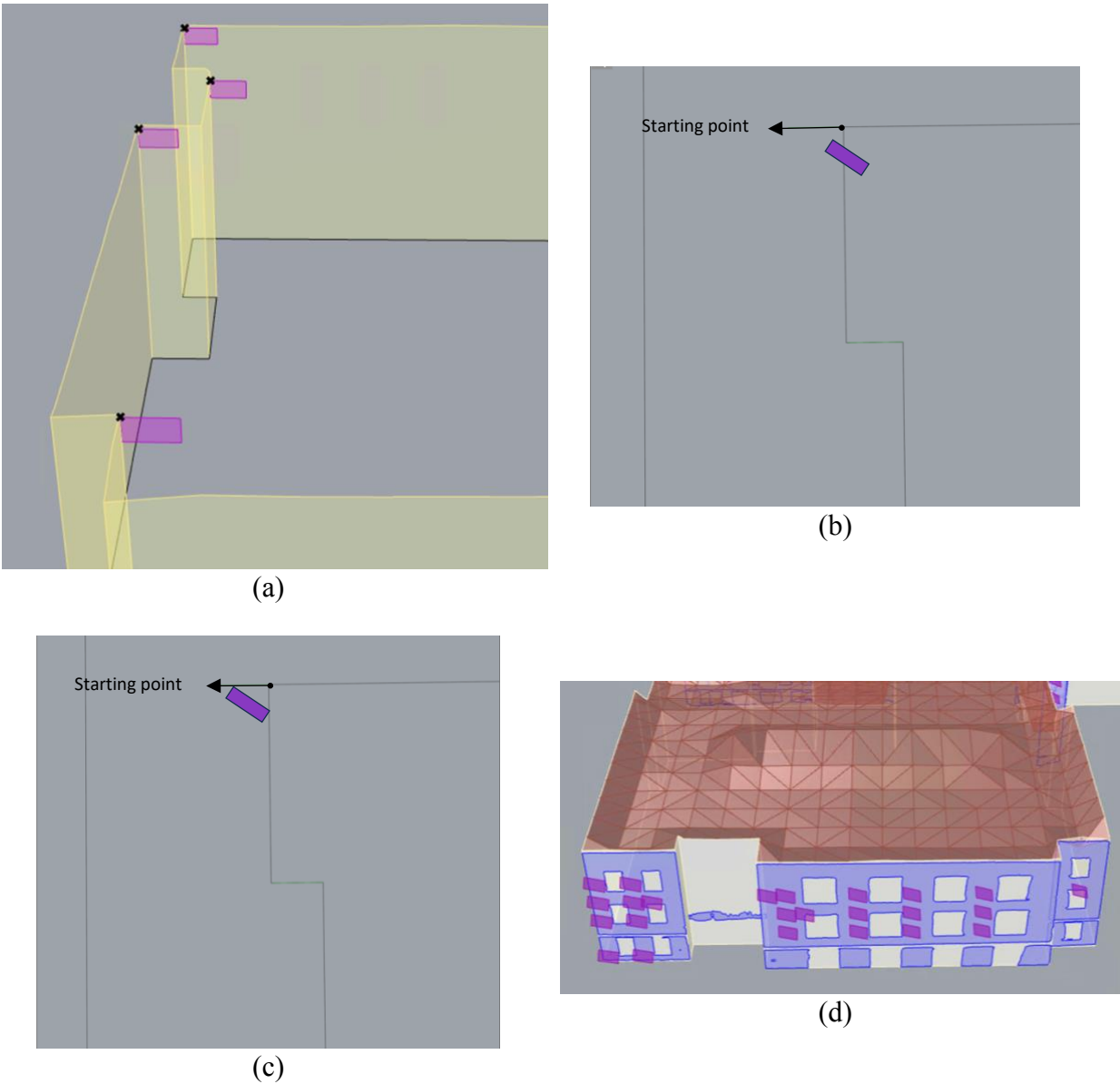


Figure 14. PV array arrangement algorithm: (a) starting points and their associated first panels; (b) PV panel oriented based on specified β , γ , and r values, from top view; (c) location readjustment of PV panels in relation to the starting point (top view) (d) final PV layout

3.5.2 Power generation of PV system

This section utilizes Ladybug tools (LBT), which is a collection of free computer applications integrated into Grasshopper, a plugin for Rhino 3D. Ladybug Tools offers a wide range of functionalities supporting environmental design and education. Among various environmental

design software packages, Ladybug Tools stands out as one of the most comprehensive options. It seamlessly integrates 3D Computer-Aided Design (CAD) interfaces with validated simulation engines such as Radiance, EnergyPlus, and OpenStudio [78], [79].

To estimate the PV system's hourly power generation over the course of a year, taking into account shading effects from surrounding objects such as nearby solar panels, trees, and neighboring buildings, LBT annual daylight simulations are performed using Radiance software. Radiance is a free and highly accurate ray-tracing software system specifically designed for lighting analysis and visualization. Unlike simpler lighting calculation and rendering tools, Radiance offers the advantage of no limitations on the complexity of geometry or materials that can be simulated [80]. Initially, the hourly solar irradiance in watts per square meter (W/m^2) is calculated using the "HD Annual Irradiance" component in LBT for the PV system [81]. This component requires inputs such as the EnergyPlus Weather File (EPW) of the building's location (Edmonton city in this study), which can be acquired from the EPW map website [82], the geometry of surrounding objects, and the PV panels.

After computing the hourly solar irradiance for the PV system in kilowatt-hours per square meter (kWh/m^2), the values are multiplied by the module area and module efficiency. Additionally, various loss factors including snow coverage, mismatch, wiring, soiling, etc., are taken into account to obtain the final hourly electricity generation of the PV system in kWh. Based on a practical study conducted by the Northern Alberta Institute of Technology (NAIT) over a four-year period, the production reduction was measured as follows: 0.25% for a tilt angle of 90° , 0.81% for 53° , 1.73% for 45° , 4.04% for 27° , 4.70% for 18° , and 4.47% for 14° [83]. To determine the snow coverage loss factor as a function of the tilt angle, a non-linear trendline technique is applied

in Microsoft Excel, as illustrated in Figure 15. Various additional loss factors are taken into consideration, as outlined in Table 4 [84].

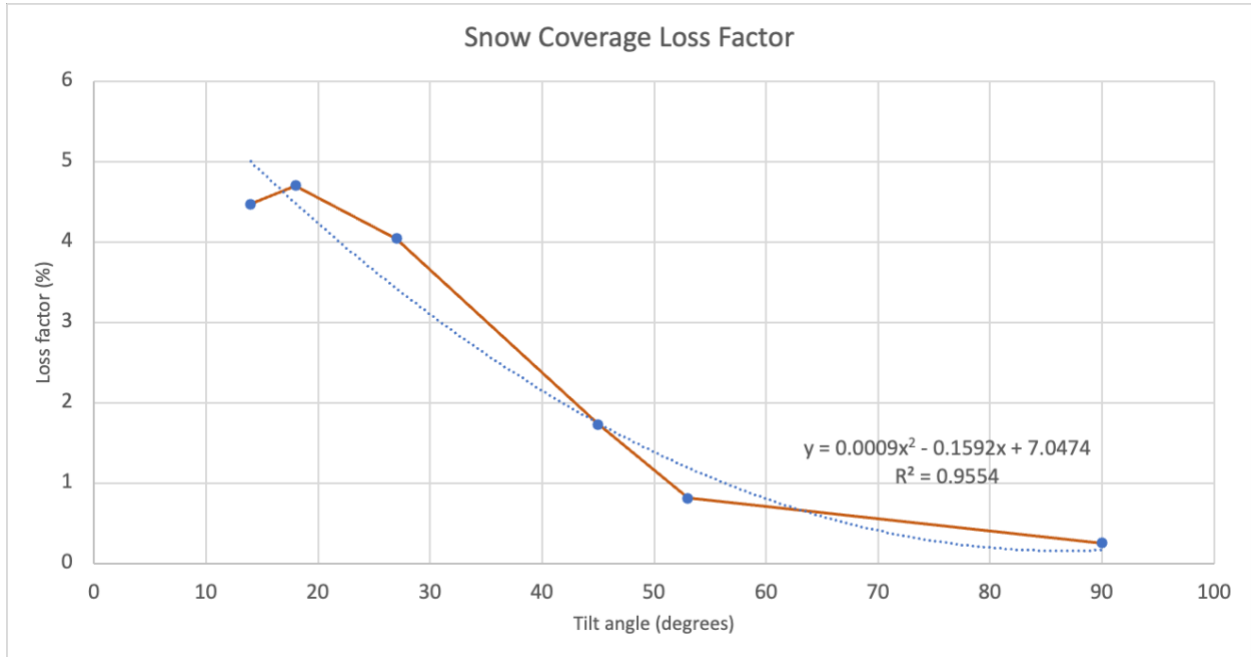


Figure 15. Snow coverage loss factors of PV generation for different tilt angles

Table 4. Estimated PV system losses (not including the snow loss factor) [84]

Parameter	Loss factor (%)
Soiling	2
Mismatch	2
Shading	3
Wiring	2
Connections	0.5
Light-induced degradation	1.5
Nameplate rating	1
Age	0.5
Availability	3
Total estimated losses (without snow loss factor)	15.5

It should be noted that in cases where the hourly power generation surpasses the maximum nominal power of the chosen panel (420W in this study), the generated power will be limited to 420W. On

another note, to enhance the efficiency of the optimization process, a panel is included in the final PV arrangement only if its generation is at least 40% of an unshaded panel with identical azimuth, tilt, and rotation angles.

3.5.3 Energy Simulation Model

To simulate the hourly energy demand of the targeted building over the course of a year, the Ladybug Tools (LBT) plugin utilizes the "HB Model to OSM" component [85]. This component is responsible for converting a Honeybee (HB) model, which represents a closed volume of the analyzed building generated in the "Simplified Building Geometry" section, into an OSM file (OpenStudio model). The OSM file can be further translated into an IDF file and run through EnergyPlus, a widely used energy simulation program.

During the simulation, the default building program for classroom and gym in OpenStudio schedules are employed for CSC and NW-VVC, respectively. These programs are used to evaluate different factors, including heating and cooling loads and daylighting performance. The results obtained from the simulation are then utilized to define the objective functions, which will be further elaborated upon in the subsequent section.

3.5.4 Objective Functions

The placement of PV modules on building façades can be approached from multiple angles, including energy efficiency, economics, and environmental impact. The most effective configuration for a PV system on building façades can vary greatly depending on the particular goal or objective. This study aims to encompass all these perspectives by integrating three distinct objectives within a multi-objective framework.

3.5.4.1 Energy-efficiency Vision

In order to assess the impact of PV system design parameters on the energy efficiency of the PV façade system, the focus is on maximizing the self-sufficiency rate (SS) of the system. SS represents the proportion of building energy consumption that is covered by the electricity generated by the system, as defined in Eq. (2) [17].

$$SS (\%) = \frac{\sum_{h=1}^{hsY} E_{con} (h)}{\sum_{h=1}^{hsY} E_L (h)} \quad (2)$$

In the given context, SS refers to the self-sufficiency rate, while $E_{con}(h)$ represents the hourly PV-generated energy specifically utilized by the building. To put it simply, if the building's demand exceeds the PV generation in a particular hour, E_{con} equals to the generated energy, and if the demand is lower, it matches the building's energy demand. $E_L(h)$ represents the hourly energy consumption of the building. These calculations are performed over the duration of one year.

3.5.4.2 Economic Factor

To enhance the economic performance of the PV system, the payback period (PB) is taken into account. This parameter indicates the number of years it takes for the total cost of purchasing and installing the PV system to be recouped through savings in electricity expenses and potential revenue from surplus solar electricity sold to the grid [38]. PB is influenced by two key factors: the initial cost (IC) and the annual revenue. The initial cost refers to the upfront investment required for the PV system and is calculated using Eq. (3).

$$IC = C_i \times N \times P_{nom} \quad (3)$$

Where C_i is the cost per installed Watt of PVs (\$/W), N is the number of panels installed in the system, and P_{nom} is the nominal power of the PV modules. In Alberta, Canada, the approximate

cost of a PV module, including all associated fees, is estimated to be around \$2.77 per Watt [86]. For the purpose of this study, the cost is approximated to be \$2.8 per Watt.

To determine the annual revenue generated by the PV system, the hourly revenue ($R(h)$) is computed using the equation provided (Eq. (4)).

$$R(h) \begin{cases} (E_G(h) - E_L(h)) \times C_s + E_L(h) \times C_b & E_G(h) \geq E_L(h) \\ E_G(h) \times C_b & E_G(h) \leq E_L(h) \end{cases} \quad (4)$$

In Eq.(4), $E_G(h)$ represents the electricity generated by a PV system within a specific hour. Additionally, the cost of purchasing electricity from the grid is indicated by C_b , while the price at which electricity is sold back to the grid is denoted by C_s . According to this equation, when the PV system generates more electricity than the hourly demand, two types of benefits can be observed. The first benefit is the cost savings achieved by not having to purchase the entire demand from the grid since it is supplied by the PV system. The second benefit is the revenue generated from selling the surplus electricity back to the grid. Conversely, if the output of the PV system is lower than the building's electricity demand, the benefit corresponds to the money saved by not having to purchase a portion of the load provided by the PV system. As per the information presented in [87], the electricity purchasing price (C_b) is uniformly set at \$0.1015 per kWh for all hours throughout the year in this particular study. Moreover, for small micro-generators with a capacity of up to 150 kW, the price at which electricity is sold to the grid (C_s) remains the same as C_b . The annual revenue (denoted as R_{annual} in Eq. (5)) can be calculated by summing up the hourly revenues for a year. It is important to highlight that the C_b calculations do not include the transmission fees [88].

$$R_{annual} = \sum_{h=1}^{hsY} R(h) \quad (5)$$

In conclusion, the calculation of the PB is determined by using Eq. (4) [87], [89]. It's pertinent to highlight that, in the present study, the annual maintenance cost and inflation rates have not been considered.

$$PB = \frac{R_{annual}}{IC} \quad (6)$$

3.5.4.3 Environmental Aspect

The environmental sustainability analysis of the PV façade system involves considering the GHG emission rate ($GHGE_{rate}$), which represents the amount of greenhouse gas emissions in grams of CO₂-equivalent per kilowatt-hour (g CO₂-eq./kWh) generated by the PV system. This metric can be obtained from the equation denoted as Eq. (7) [9], [39], [90].

$$GHGE_{rate} = \frac{GHG_{PV} + GHG_{BOS}}{E_{LCA-output}} \quad (7)$$

The total GHG emissions of the PV module are denoted as GHG_{PV} , while GHG_{BOS} represents the total GHG emissions from the balance of system components. Additionally, $E_{LCA-output}$ refers to the electric power produced by the PV system, measured in kWh. In order to determine the value in the numerator of the mentioned equation, two factors are taken into account. First, the average primary energy input of the PV module over its entire life cycle, which encompasses energy requirements for manufacturing, transportation, installation, operation and maintenance, and recycling, is denoted as E_{input} . Second, the energy required for the physical balance of system (BOS), including mounting structures, cabling, electronic components, and inverters, is

represented as E_{BOS} (both measured in MJ/m²). E_{input} and E_{BOS} are derived from a compilation of various studies, as summarized by Peng et al. (2013) [90] in Table 5.

Table 5. Overview of the energy-related data pertaining to the life cycle of polycrystalline solar panels

E (MJ/m²)	Min	Max	Average
input	2699	5150	3925
BOS	500	2030	1265

Afterwards, these factors are multiplied by the width (w_m) and length (l_m) of PV modules, number of panels (N), the average GHG emission rate of a PV panel over its lifecycle ($GHGE_{LC-rate}$), which is approximately 46 g per kWh [91], and the conversion factor from Joule to Watt to compute GHG_{PV} and GHG_{BOS} , as presented in Eq. (8).

$$GHG_{PV}, GHG_{BOS} (g) = E_{input}, E_{BOS} \left(\frac{MJ}{m^2} \right) \times l_m (m) \times w_m (m) \times N \times GHGE_{LC-rate} \left(\frac{g}{kWh} \right) \times \frac{1 kWh}{3.6 \times 10^6 J} \quad (8)$$

To determine $E_{LCA-output}$, the total yearly electricity generation of the PV system is multiplied by the operational years of the PV panel (Y_o), which is assumed to be 25 years in this study. This calculation is represented by the following equation.

$$E_{LCA-output} (kWh) = \sum_{h=1}^{hsY} E_L (h) \times Y_o \quad (9)$$

3.5.5 Multi-Objective Optimization of PV Layout

As previously discussed, the optimization process considers three distinct objective functions: maximizing SS to improve energy-efficiency, minimizing PB for economic considerations, and minimizing $GHGE_{rate}$ to address environmental aspects. This approach creates a multi-objective

platform aimed at identifying the most appropriate PV layout. To carry out the optimization process, the Wallacei plugin is used. Wallacei is an evolutionary engine designed to run simulations within Grasshopper 3D. It offers highly detailed analytic tools and incorporates comprehensive selection methods. This combination helps users gain a deeper understanding of their evolutionary simulations and make well-informed decisions at all stages of the process. Wallacei primarily utilizes the NSGA-2 algorithm as the main evolutionary algorithm [92], [93]. It's worth noting that there are alternative optimization plugins like Octopus. However, Wallacei stands out as it is compatible with the latest versions of Rhino software, unlike some other plugins that have not been updated to newer versions. Since Wallacei is designed to minimize any given objective, in order to maximize SS , it is multiplied by -1. To summarize, the objective functions can be expressed as follows:

$$\text{Minimize } [-SS(L_h, L_v, \beta, \gamma, r), PB(L_h, L_v, \beta, \gamma, r), GHGE_{rate}(L_h, L_v, \beta, \gamma, r)] \quad (10)$$

The optimization algorithm is applied individually to the vertical faces of each façade, namely the south, west, and east façades. In this approach, the south-facing vertical faces are grouped together, and the optimization process is then repeated for the west-facing and east-facing surfaces separately. To tailor the optimization process for each façade based on solar irradiance patterns and ensure more logical SS calculations, specific time periods are considered for different orientations. For east-facing façades, the optimization focuses on the PV generation and energy demand in the first 50% of the total daytime hours throughout the year. For south-facing façades, the middle 50% of daytime hours are taken into account, while the last 50% is considered for west-facing façades. We opted for this method because all the analyzed building facades align with cardinal directions. However, if a facade, for instance, faces southeast, the chosen daytime hours would need to be adapted accordingly. The order of optimization for façades is determined by

simulating solar irradiance on three identical imaginary panels placed on east, west, and south-facing façades. It was observed that the south-facing panel received the highest solar irradiance, while the east-facing panel received the lowest. Therefore, the optimization is first conducted for the south-facing façades, followed by the west and east-facing façades. To ensure coherence between the optimization of different façades, the hourly generation of the selected optimal layout is subtracted from the hourly energy demand of the building data each time we move to optimize a different part of the same building. This ensures that, for instance, if the PV panels on the south-facing façades already cover the required energy demand for a specific hour, the optimization for the west-facing part will not attempt to add extra PV panels unnecessarily due to the demand already being met in the previous optimization step.

Chapter Four: Results & Discussion

Within this chapter, the results obtained from applying various stages of the proposed methodology to the case study buildings, CSC and NW-VVC, are provided. Initially, the simplified building geometries are showcased. Following this, the outcomes of the CNN model training, along with examples of predicted segmented masks, are displayed. Subsequently, the developed methodology and employed approaches are validated. Lastly, the optimization results for each façade orientation of the case study buildings are presented and analyzed.

4.1 Simplified Building Geometries

As discussed in the preceding chapter, the initial and primary phase of implementing the developed approach involves simplifying the building meshes imported from the Google Maps 3D models. Figure 16 and Figure 17 depict the simplified and recreated geometries for the case study buildings. The simplified façade surfaces are visualized in yellow, while the recreated roof meshes are displayed in red.

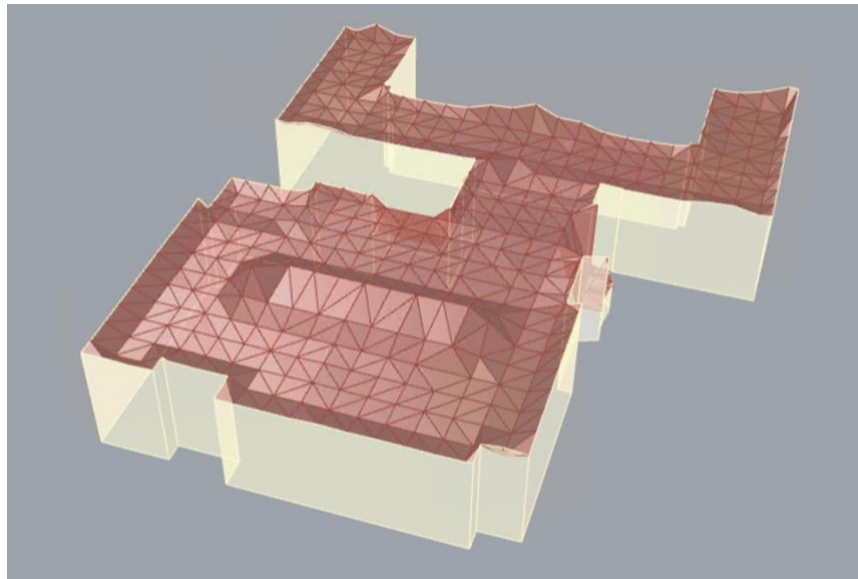


Figure 16. Simplified geometry of CSC

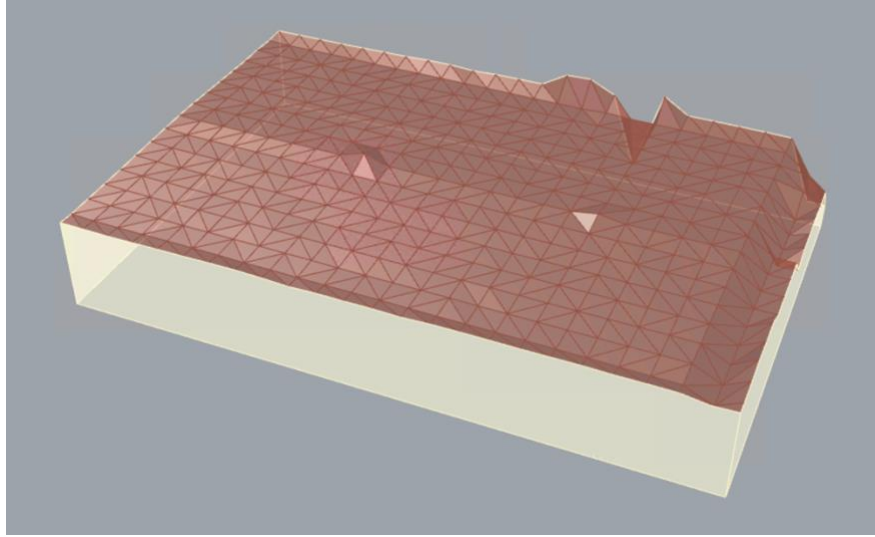


Figure 17. Simplified geometry of NW-VVC

As depicted in Figure 16, the geometry of the CSC building is connected to Athabasca Hall. This decision was made because their footprints are contiguous, and it also allows for the inclusion of a case study building with all its façade orientations available for solar panel installation. On the contrary, Figure 17 shows NW-VVC with a simpler rectangular footprint. Moreover, since the east façade of NW-VVC is attached to a neighboring building, it is excluded from the optimization process.

4.2 Façade Segmentation Results

In this section, the dice loss and IoU scores for the training and validation sets of the façade segmentation dataset during the training of the CNN model in each epoch are displayed. Additionally, the results of predicting the images from the test set using the final saved model are presented. Moreover, given the high number of façade parts in the case studies, a few of them are selected to showcase their predicted mask results generated by the trained deep learning model.

4.2.1 CNN Model's Training Results

The CNN model is trained using a single NVIDIA A100-SXM4 GPU with 40 GB of memory. Utilizing a training batch size of 16 effectively capitalizes on the GPU's parallel processing capabilities, resulting in faster training times. This approach facilitates efficient computation and smoother gradient updates during the training process. On the other hand, for the validation set, a smaller batch size of 8 can still yield a representative evaluation of the model's performance. This choice strikes a reasonable balance between computational efficiency and obtaining reliable performance metrics. Unlike the training phase, the validation batch size doesn't involve backpropagation and parameter updates, making it unnecessary to be as large as the training batch size. In summary, a batch size of 16 for training and 8 for validation is a commonly adopted and practical configuration, ensuring both computational efficiency and accurate performance evaluation. In accordance with the information provided earlier, the façade segmentation model undergoes training for a total of 70 epochs. During each epoch, the model's weights are saved if the IoU score of the validation set surpasses the IoU score obtained in the previous epochs. Figure 18 showcases the progression of the loss values over the course of the training process and offers insights into how the model performs on both the training and validation datasets at each epoch. The plot demonstrates a consistent and stable convergence pattern during both the training and validation processes. Notably, as the training progresses, the loss for both the training and validation sets steadily decreases and converges to a low value after approximately 30 epochs. Moreover, the Mean IoU values for both the training and validation datasets exhibit significant improvement and reach high values after 30 epochs, as illustrated in Figure 19. This indicates that the developed approach demonstrates a swift convergence speed and maintains high stability

during the training process. In conclusion, the model effectively learns to segment façades, making it a reliable and robust solution.

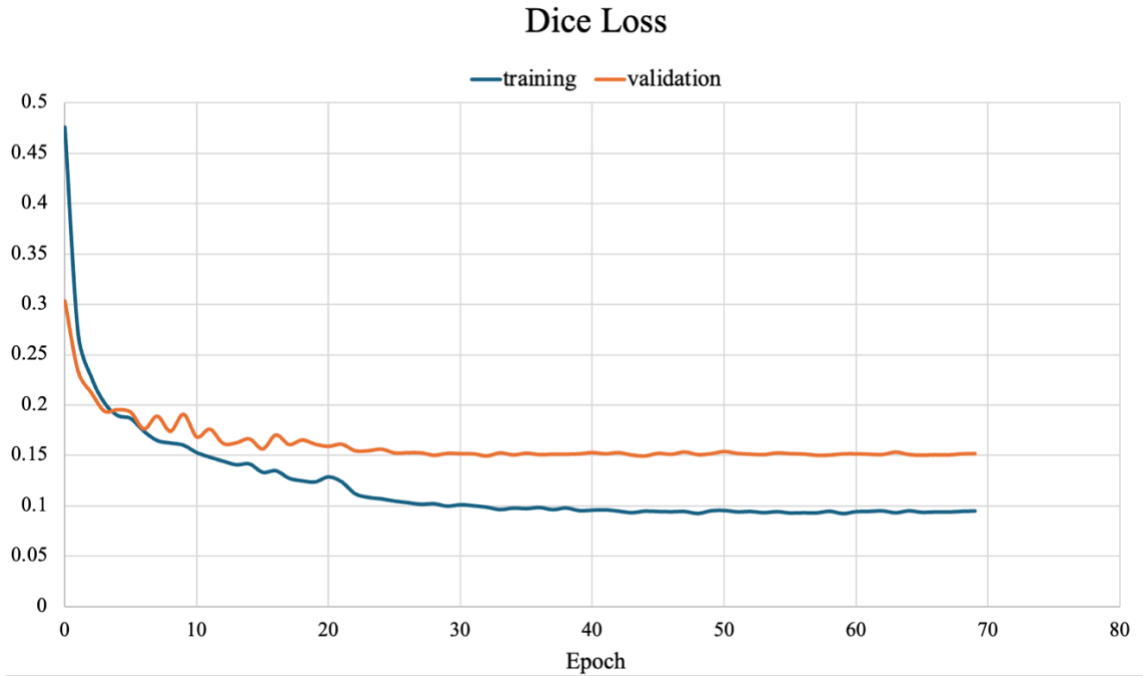


Figure 18. Training and validation loss during CNN model training

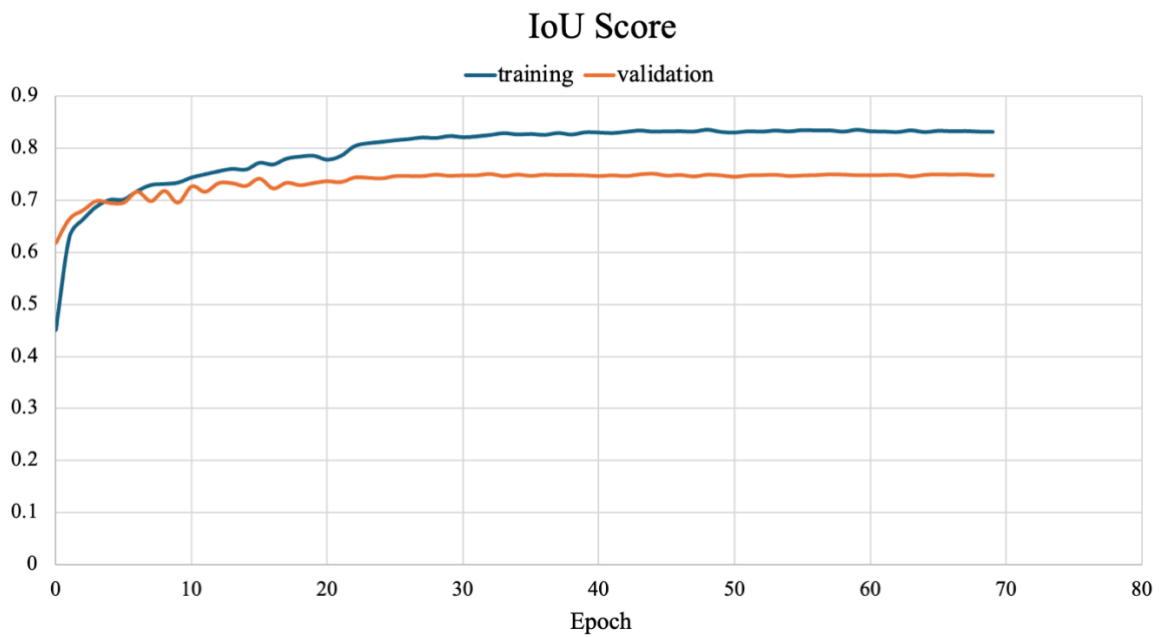


Figure 19. Training and validation IoU during CNN model training

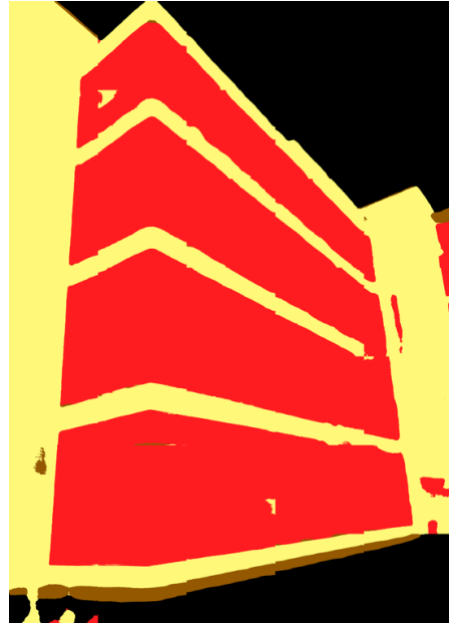
After utilizing the final saved model to perform segmentation on the test set, a comprehensive evaluation of its overall performance is conducted. The outcomes are subsequently summarized in Table 6. The results of the model showcase a performance that is consistent with the façade parsing models found in the existing literature.

Table 6. Performance evaluation of the segmentation model on the test set

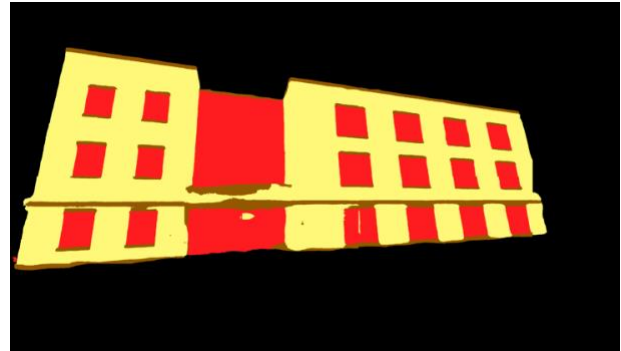
Evaluation Metric	Value
Mean IoU	0.81
Mean dice loss	0.13
F1 score	0.88
Accuracy	0.96
Recall	0.87
Precision	0.88

4.2.2 Samples of Predicted Masks

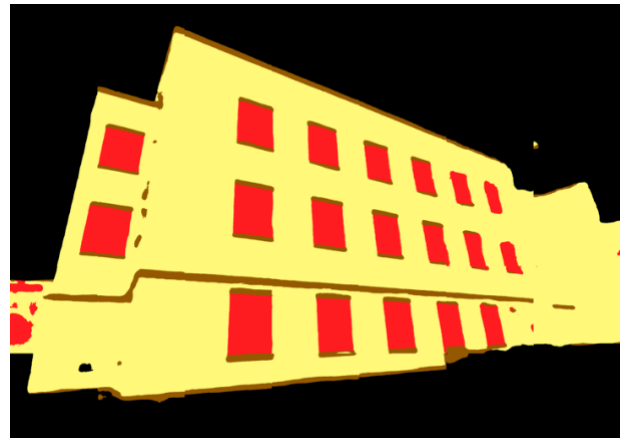
In this section, a selection of classified façade images using the final saved model is presented in Figure 20. The model demonstrates favorable performance in predicting various façade elements. However, it encounters challenges when dealing with parts of façades occluded by vegetation and other smaller obstacles situated in front of the building. Notably, recent works in the field of computer vision have focused on devising diverse deep learning networks with multiple branches to tackle this specific issue.



(a)



(b)



(c)

Figure 20. Examples of the segmented façades with trained CNN: (a) University of Alberta Observatory; (b) West side of CSC; and (c) South side of CSC

4.3 Combined 2D Segmented Masks with 3D Models

Once the segmented masks for all the façades of the case study buildings are acquired, they undergo a perspective transformation or rectification process. As a simplification step, the colors of various façade elements in the rectified masks are transformed to create black & white images. In these images, the wall parts that are suitable for PV installation are displayed in white, while the remaining parts are displayed in black, indicating that they are not suitable for installation. Due to the considerable number of façade parts, only a few of them are showcased here as examples.

4.3.1 Rectified & Processed Segmented Masks

As previously discussed, the process of rectifying each façade image involves selecting the four corners of the vertical face in a clockwise order, starting from the top-left corner, as determined by the user. The height and length of the specific building face are then derived from the Google Earth platform and used as inputs for the perspective warping function in the OpenCV library. Figure 21 presents a collection of samples demonstrating the outputs of the segmentation model: the rectified masks on the left side and the corresponding filtered black and white masks on the right side.

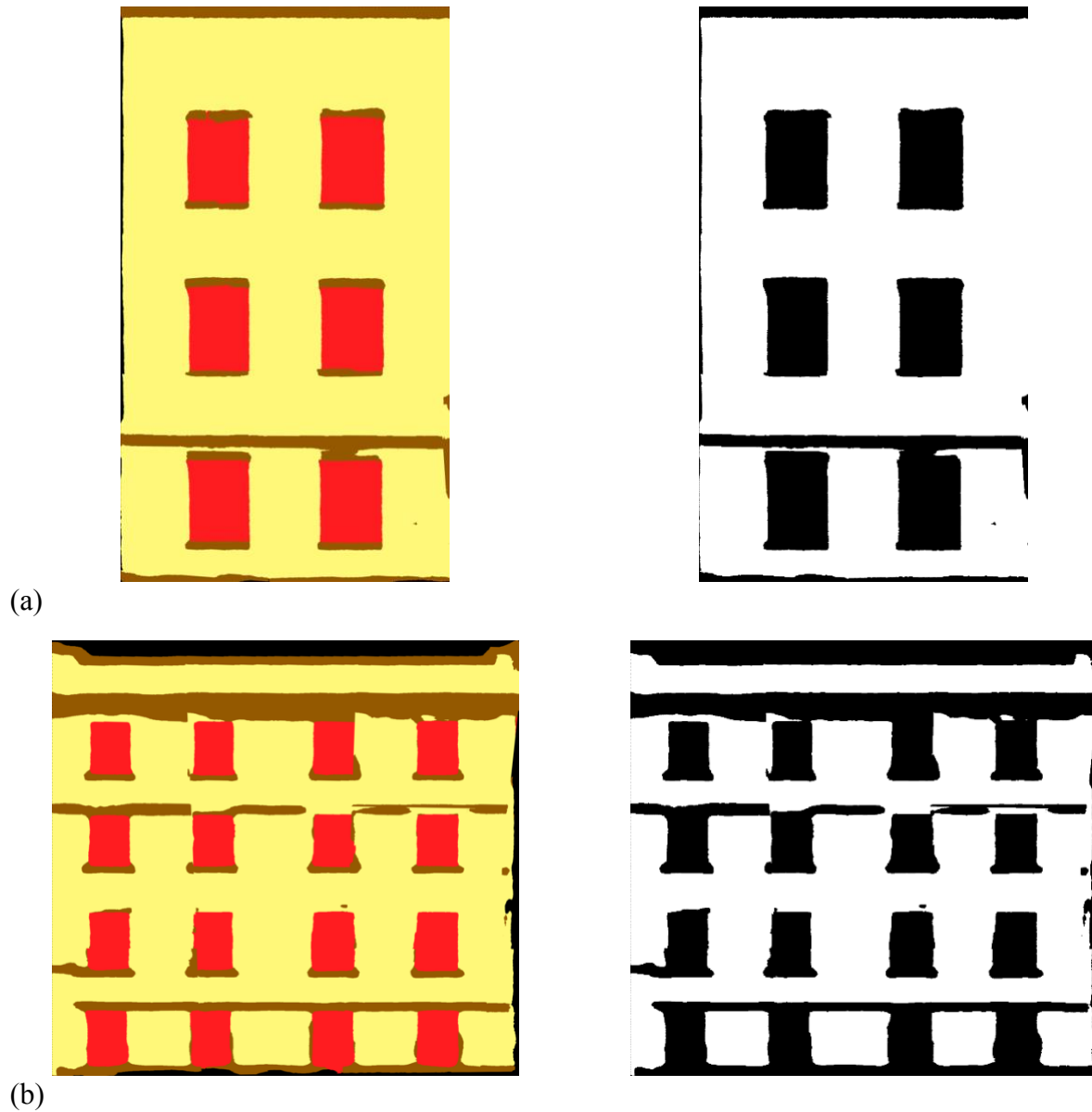


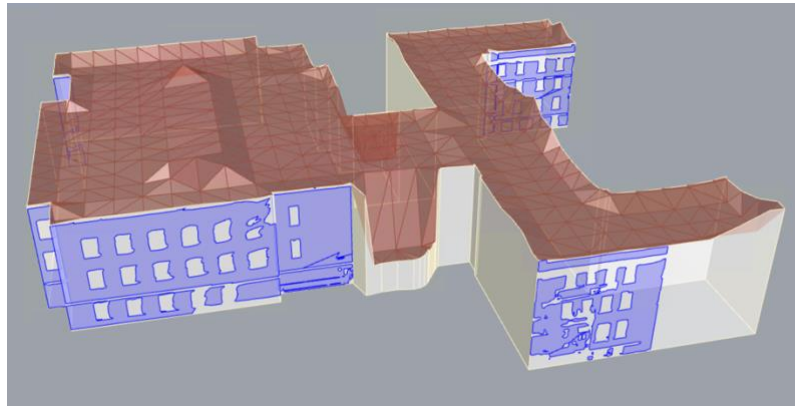
Figure 21. A selection of rectified and filtered segmented masks: (a) CSC, west façade; (b) CSC, south façade

It is essential to emphasize that instead of inputting the actual dimensions of the building face, users have the option to input approximate correct ratios using the original image. For instance, if the height of the given face is noticeably longer than its length and approximately two times more, the user should consider this when inputting the dimensions of the given face. When using the

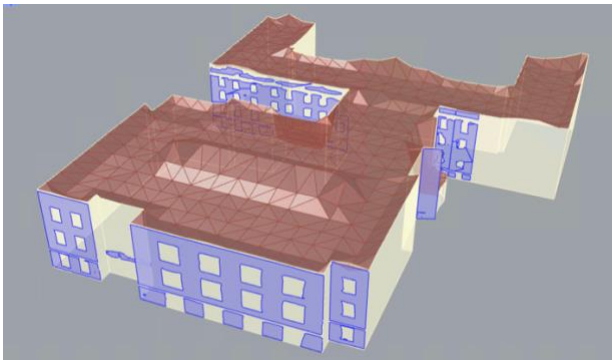
rectangle mapping component in Grasshopper, these dimensions will be automatically adjusted to fit the filtered rectified mask within its corresponding vertical surface area in the 3D model of the building. This enables a seamless integration of the filtered rectified mask with the building's 3D model, providing a more accurate representation of the PV installation areas.

4.3.2 Projected Mask onto Façades

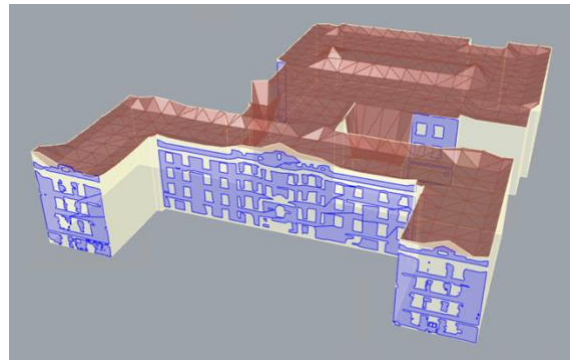
Once the façade masks are rectified and filtered, they are imported and projected onto their corresponding vertical surfaces, as explained in the previous chapter. In Figure 22, only the white parts from the filtered masks, which represent the wall sections of the façades, are projected onto the surfaces. In Figure 22, the projected areas are highlighted in blue, offering a distinct visual representation of the regions that are ideal for PV installation on the façades of the case study buildings. To clarify the process, these highlighted areas serve as projected masks during the optimization. This means that panels are initially projected onto the respective vertical surface of the building where they will be placed. Subsequently, if this projected geometry falls within the blue regions, the panel is taken into consideration for the optimization process to determine the final PV layout.



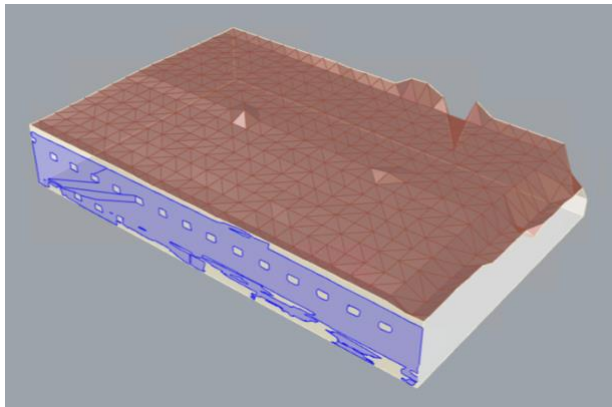
(a)



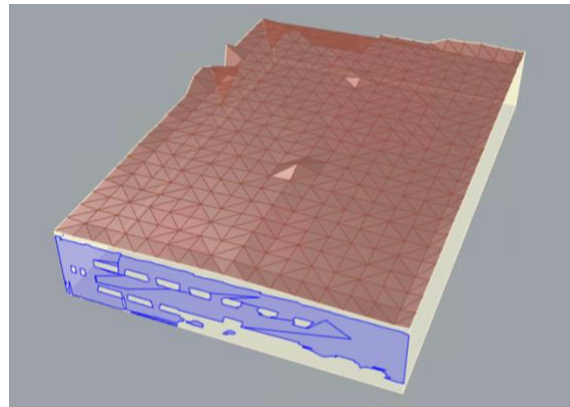
(b)



(c)



(d)



(e)

Figure 22. Projected final masks on the façades of the case study buildings: (a) CSC, south façade; (b) CSC, west façade; (c) CSC, east façade; (d) NW-VVC, south façade; (e) NW-VVC, west façade

The PV layout algorithm is specifically designed to eliminate panels that fall outside the blue areas on the façades in the 3D model. It exclusively considers the panels placed within those areas for

the optimization process. This approach ensures that only the wall parts of façades, represented by blue regions, are taken into account when optimizing the placement of PV panels on the building façades. As depicted in the displayed images, the areas of the façades that are heavily obscured by trees have been marked in black to indicate that they will not be taken into consideration for PV installation.

4.4 Framework Validation

As mentioned earlier, LBT is based on well-established simulation engines such as Radiance, EnergyPlus, and OpenStudio. Its validation has been successfully accomplished through several previous papers, providing a reliable basis for utilizing this tool in the PV generation model and energy simulation [94]–[96].

To further evaluate and validate the developed framework, the PV generation of a single panel with the same PV module settings as mentioned in Table 3 is calculated for the south-facing orientation ($\gamma=0^\circ$) with a tilt angle (β) of 50° in Edmonton. According to data from Natural Resources Canada, the average solar system in Alberta can produce 1276 kWh of electricity per kW of solar panels per year [86]. The annual electricity generation of the panel, using the formula mentioned in the "Power generation of PV system" section, is estimated to be 562.54 kWh assuming no shading effects from surrounding objects. Given that the nominal power of the panel is 420 W, this indicates that the panel can produce 1339.38 kWh of electricity per kW of solar panel. The difference between the results obtained in this research and the data provided by Natural Resources Canada is 4.97%, which is within an acceptable range of deviation.

4.5 Optimization Results

As previously mentioned, the multi-objective optimization is conducted using the Wallacei plugin. The optimization algorithm settings, which are consistent for all façades and case study buildings, are outlined in Table 7. Moving forward, the subsequent sections delve into an in-depth presentation and discussion of the detailed results obtained during the process of determining the optimal PV layout variables for each façade orientation in both case studies. These discussions aim to provide a comprehensive understanding of the findings and their implications for the overall performance and efficiency of the PV systems on the buildings' façades.

Table 7. Settings of optimization algorithm

Parameter	Value
Generation size	20
Generation count	80
Crossover probability	0.89
Mutation probability	1/n
Crossover distribution index	20
Mutation distribution index	20
Random seed	1

4.5.1 CSC

The CSC building's façades consist of various faces, with the curve-shaped portion of the footprint excluded from PV placement considerations. Furthermore, the sections of the façades that completely fall within the uninstallable areas for PV are also disregarded. Additionally, as mentioned previously, any parts of the façades that are fully obscured by trees are not taken into account. Moreover, the minimum length of each façade part must be greater than the longest dimension of the PV module, which is 2.05 m. Taking all these factors into consideration, the south façade is comprised of 6 faces, the west-facing façade has 6 parts, and the east-facing façades have 5 parts. In the subsequent sections, the optimization results for each façade orientation will be

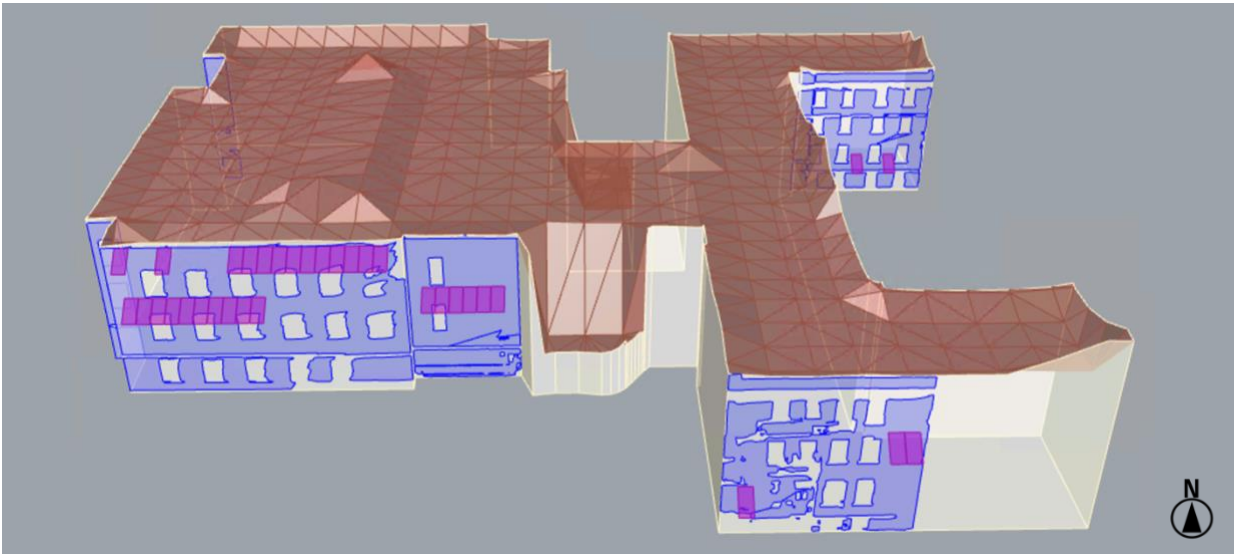
presented and discussed. These results shed light on the most effective PV layout variables for each specific façade orientation, providing valuable insights for maximizing the PV system's efficiency on the building façades. Furthermore, the EnergyPlus simulation estimates the total annual energy demand of this building to be approximately 1164028.58 kWh.

4.5.1.1 South

The optimized PV layout consists of 34 panels, collectively capable of generating up to 16611.83 kWh of electrical energy over the course of a year. As previously mentioned, the *SS* for optimizing the PV system on the south façade is calculated for the 50% middle sunlight hours of each day. For instance, if the sun rises at 9 am and sets at 5 pm on a winter day, the PV generation of the system and the building's load used in the *SS* calculation for optimization are considered from 11 am to 3 pm. The values for the remaining hours are multiplied by 0 in the *SS* calculation, aligning the optimization process with the sun patterns and taking into account the influence of other façades' PV systems on the optimization of this specific façade. The optimal PV arrangement settings are provided in Table 8, while Figure 23a illustrates its visualization.

Table 8. PV design parameters for the south façade of CSC building

PV design parameter	Value
L_h	0.0 m
L_v	3.0 m
β	40°
γ	0°
r	90°



(a)



(b)

Figure 23. (a) Optimum PV layout for the south façade of CSC building; (b) South façade of CSC building in Google's 3D model (Imagery ©2023 Google, Imagery ©2023 CNES / Airbus, Maxar Technologies, Map data ©2023 Google)

As shown in the above illustration, it is evident that particular parts of the façade experience inadequate segmentation. As demonstrated in Figure 23b, this discrepancy can be traced back to the existence of a staircase on the right and trees on the left. In general, further examination of the

results in these specific segments is required, along with the possible improvement of the CNN model in future attempts. As observed in the figure above, on the lower left side of the building's larger façade, there is a continuous, light brown obstacle that has caused the distance between the second and third windows (from top to bottom) to be shorter than the distance between the first and second ones. Consequently, this region does not provide enough space for the placement of panels. Furthermore, on the top section of the larger façade, there exists a space between the panels. This occurs because the upper edge of the mask is not perfectly straight, causing small portions of the panels to extend beyond the blue region. Consequently, these panels are excluded from the PV layout taken into account for optimization. It is worth noting that the shading resulting from the obstacles and trees makes it likely that the optimization process will avoid placing panels in certain regions as well. The achieved objective function values for the optimized PV layout are as follows: 6.03% for *SS*, approximately 24 years for *PB*, and 11.98 g CO₂-eq./kWh for *GHGE_{rate}*.

4.5.1.2 West

The optimal PV layout for the west façade of the building incorporates 62 solar panels, which together can produce 21631.67 kWh of electrical energy annually. To address any potential overlap of sunlight hours between the south and west façades in the *SS* calculation during the west façade's optimization, a specific strategy is implemented. To avoid installing unnecessary PV panels on the west façade due to the south-facing PV system already meeting a portion of the building's energy demand, the hourly electricity generation produced by the optimal south-facing PV system is subtracted from the total hourly energy demand of the building. Any negative values resulting from this subtraction (when generation exceeds demand) are set to zero. Following this, the *SS* calculation for the west façade is focused on the second half of the daytime hours in each day throughout the year. For instance, considering the example provided in the previous section where

the sun rises at 9 am and sets at 5 pm, the PV generation and building load used for the *SS* calculation during west façade optimization are considered from 1 pm to 5 pm. The values for the remaining hours are multiplied by 0 in the *SS* calculation, highlighting the impact of solar irradiance during the afternoon and evening hours in the optimization process. This approach ensures that the PV system on the west façade is optimized based on specific sunlight conditions and energy demand patterns during the afternoon and evening, resulting in an efficient and effective PV layout for this particular façade. The optimal PV arrangement settings for the west façade are provided in Table 9, offering valuable insights into how the panels are positioned and configured to achieve the desired results. Additionally, Figure 24 visually illustrates the visualization of this optimized PV layout on the west façade, providing a clear representation of the panel placements and their integration into the building's architecture.

Table 9. PV design parameters for the west façade of CSC building

PV design parameter	Value
L_h	0.0 m
L_v	0.5 m
β	50°
γ	30°
r	135°

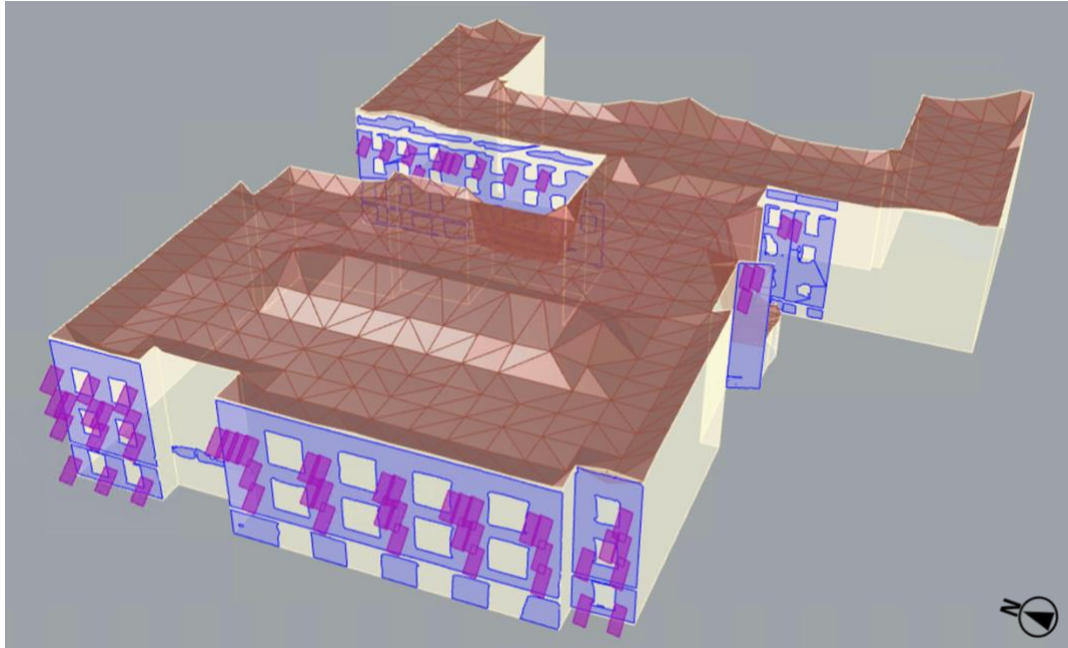


Figure 24. Optimum PV layout for the west façade of CSC building

The resulting objective function values for the optimized PV layout are as follows: *SS* of 6.38%, *PB* of approximately 33 years, and a $GHGE_{rate}$ of 16.79 g CO₂-eq./kWh.

4.5.1.3 East

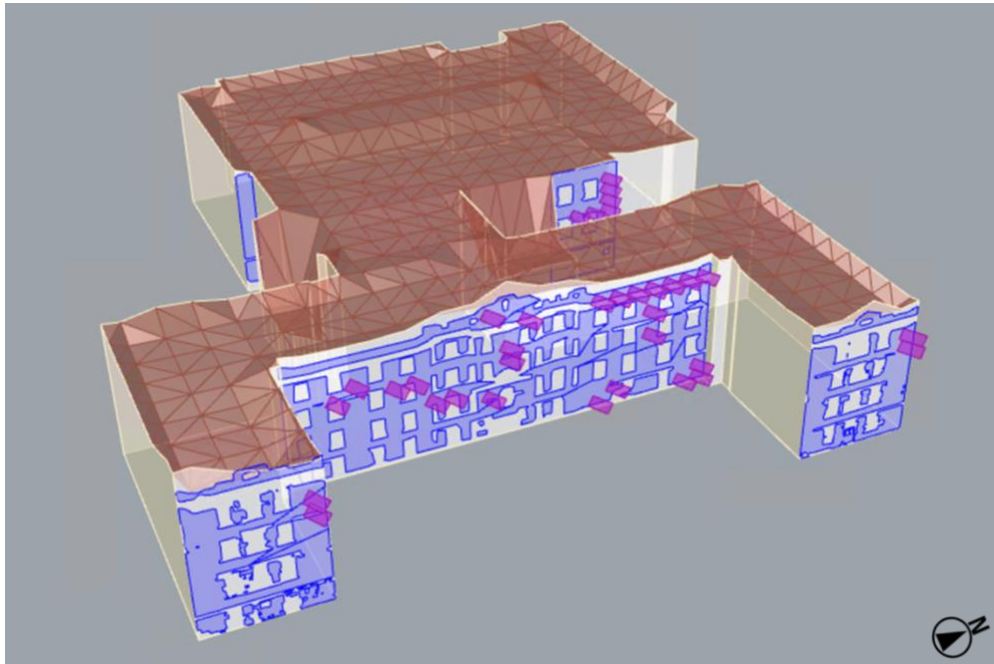
After completing the optimization process for both the south and west façades, the next façade to be optimized is the east façade. The optimal configuration for this specific façade comprises 35 PV panels, generating a total of 11214.46 kWh of energy annually. Like the previous sections, the optimization for the east façade also takes into consideration the potential overlap of sunlight hours between the south and east façades in the *SS* calculation. Additionally, it ensures that unnecessary PV panels are not installed on the east façade due to the south-facing and west-facing PV systems already fulfilling a portion of the building's energy demand. To achieve this, the hourly electricity generation produced by the optimal south-facing PV system and the hourly electricity generation produced by the optimal west-facing PV system are summed, and the total is then subtracted from

the total hourly energy demand of the building. Any resulting negative values are set to zero, ensuring an accurate and efficient optimization process. Subsequently, the *SS* calculation for the east façade focuses on the first half of the daytime hours in each day throughout the year. For example, considering the previous example where the sun rises at 9 am and sets at 5 pm, the PV generation and building load used for the *SS* calculation during the east façade optimization are considered from 9 am to 1 pm. The values for the remaining hours are multiplied by 0 in the *SS* calculation, emphasizing the impact of solar irradiance during the morning and noon hours in the optimization process. This approach ensures that the optimization for the east façade is tailored to specific sunlight conditions and energy demand patterns during the morning and early afternoon, leading to an effective PV layout specifically designed for this façade. The optimum PV arrangement settings for the east-facing façade are presented in As illustrated in Figure 25b, akin to the observations made for the southern façade, it becomes apparent that specific segments of the façade display inaccuracies in the classification of predicted masks. This inconsistency emerges due to the diverse array of façade elements present, compounded by the obstruction created by trees.

Table 10, showcasing the strategic positioning and configuration of the PV panels to maximize efficiency. A visual representation of this optimized PV layout on the east façade is depicted in Figure 25a. These findings offer valuable insights into the effective utilization of solar energy on the east-facing façade, contributing significantly to the overall energy efficiency and sustainability of the building. As illustrated in Figure 25b, akin to the observations made for the southern façade, it becomes apparent that specific segments of the façade display inaccuracies in the classification of predicted masks. This inconsistency emerges due to the diverse array of façade elements present, compounded by the obstruction created by trees.

Table 10. PV design parameters for the east façade of CSC building

PV design parameter	Value
L_h	0.0 m
L_v	0.5 m
β	40°
γ	-30°
r	0°



(a)



(b)

Figure 25. (a) Optimum PV layout for the east façade of CSC building; (b) East façade of CSC building in Google's 3D model (Imagery ©2023 Google, Imagery ©2023 CNES / Airbus, Maxar Technologies, Map data ©2023 Google)

The optimized PV layout achieved the following objective function values: a SS of 3.08%, a PB of approximately 36 years, and a $GHGE_{rate}$ of 18.29 g CO₂-eq./kWh.

In general, when considering the entire building and summing up the hourly generation of the optimized PV systems for each façade, the SS rate is calculated to be approximately 3.52%. This indicates that the PV systems are able to meet around 3.52% of the building's total energy demand. The total PB for the optimized PV layouts is estimated to be approximately 31 years. This means that it would take around 31 years for the cumulative energy savings from the PV systems to offset the initial investment cost. Regarding the $GHGE_{rate}$, it is found to be 15.52 g CO₂-eq./kWh. This value represents the amount of greenhouse gas emissions associated with generating 1 kWh of electricity using all the optimal PV systems. Overall, these results demonstrate the energy efficiency and environmental benefits of the optimized PV layouts, as it contributes to reducing the building's reliance on external energy sources and lowering its carbon footprint over time.

4.5.2 NW-VVC

Given the rectangular shape of NW-VVC building's footprint, each façade orientation comprises only one face. Due to the east façade being attached to and obscured by a neighboring building, the PV installation optimization process is first focused on the south façade and subsequently on the west façade. According to the EnergyPlus simulation, the total annual energy demand of this building is approximately 808634.26 kWh. The following sections will provide a detailed presentation and discussion of the optimization results for each façade orientation.

4.5.2.1 South

The optimized PV layout for the south façade of NW-VVC building consists of a total of 121 panels, generating approximately 56324.64 kWh of electrical energy annually. As with the CSC

building, SS for optimizing the PV system on the south façade is calculated based on the 50% middle sunlight hours of each day. Table 11 provides detailed information about the optimal layout variables, while Figure 26 visually presents the placement and configuration of the panels on the south façade, offering a clear representation of their integration into the building's design.

Table 11. PV design parameters for the south façade of NW-VVC

PV design parameter	Value
L_h	0.0 m
L_v	0.5 m
β	60°
γ	0°
r	0°

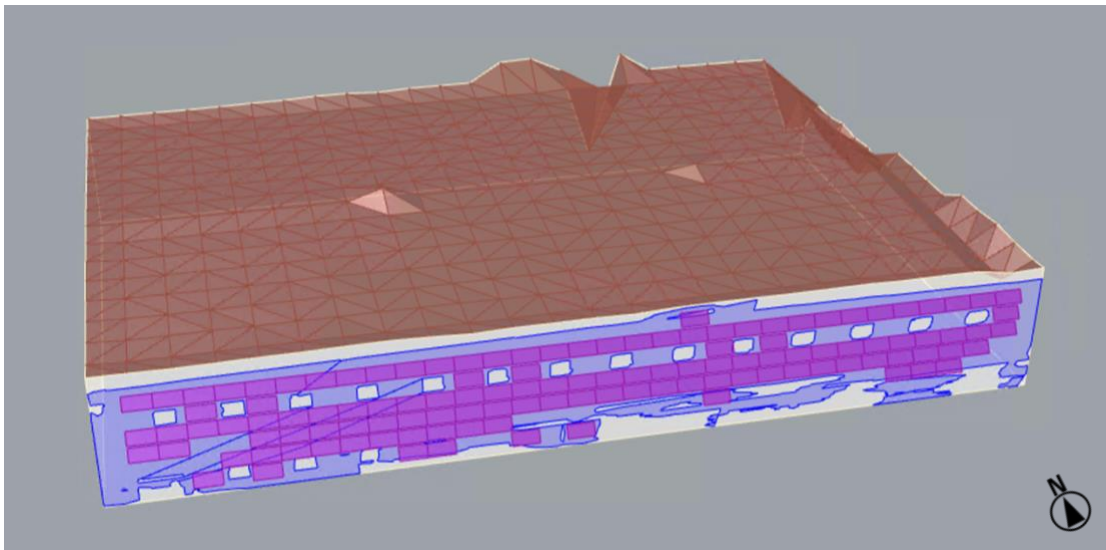


Figure 26. Optimum PV layout for the south façade of NW-VVC

The optimization process resulted in the following objective function values for the optimized PV layout: a SS of 23.28%, a PB of around 25 years, and a $GHGE_{rate}$ of 12.59 g CO₂-eq./kWh.

4.5.2.2 West

The west façade's optimal PV layout involves 88 solar panels, capable of producing an annual energy output of 30982.65 kWh. To ensure accurate results, the *SS* calculation for the west façade considers potential overlap of sunlight hours with the south-facing façade. By subtracting the hourly electricity generation from the optimal south-facing PV system from the total hourly energy demand of the building, any negative values are set to zero. The optimization process focuses on the second half of the daytime hours throughout the year, aligning with the afternoon sunlight conditions. Table 12 presents the specific PV arrangement settings, providing valuable insights into how the panels are positioned and configured for optimal performance on the west façade. In addition, Figure 27 provides a visual representation of the optimized PV layout on the west façade. The optimization process yielded the following objective function values for the optimized PV layout: a *SS* of 12.95%, a *PB* of around 33 years, and a *GHGE_{rate}* of 16.64 g CO₂-eq./kWh.

Table 12. PV design parameters for the west façade of NW-VVC

PV design parameter	Value
L_h	0.5 m
L_v	0.0 m
β	60°
γ	60°
r	0°

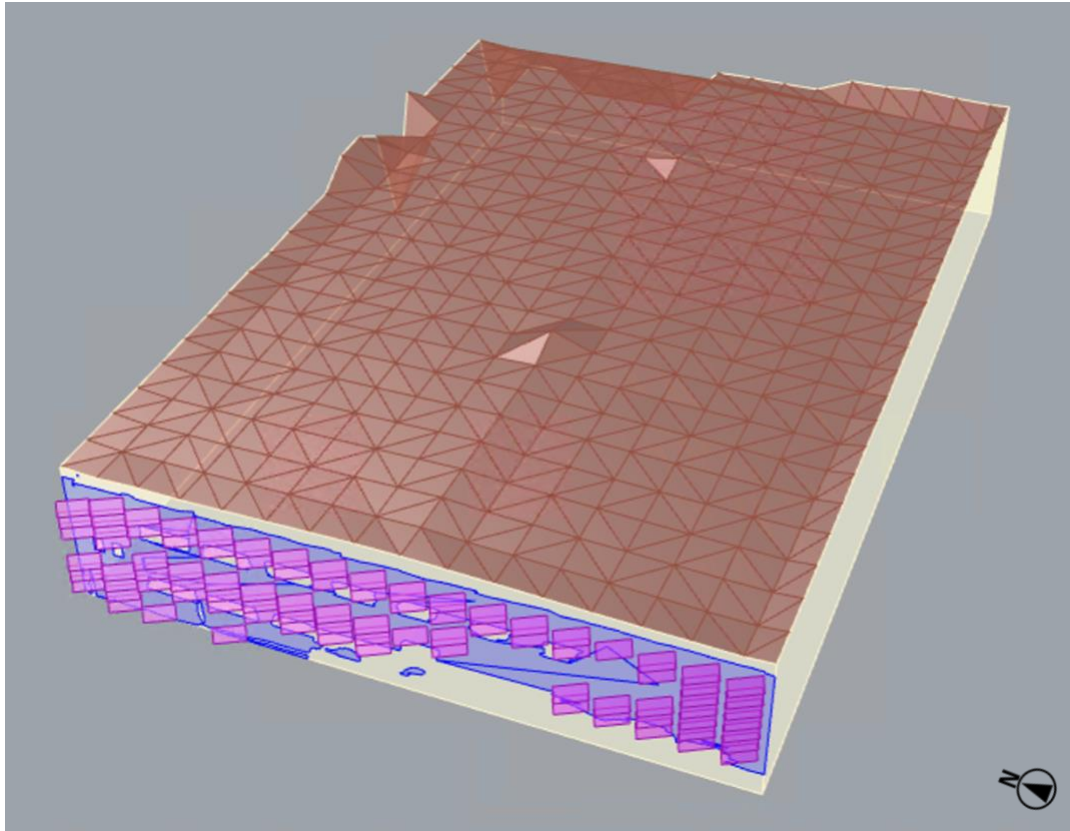


Figure 27. Optimum PV layout for the west façade of NW-VVC

In summary, taking into account the entire building and aggregating the hourly generation of the optimized PV systems for each façade, the overall SS is approximately 8.59%. The total PB for the optimized PV layouts is estimated to be around 28 years. As for the $GHGE_{rate}$, it is calculated to be 14.03 g CO₂-eq./kWh, indicating the amount of greenhouse gas emissions linked to generating 1 kWh of electricity using the optimized PV systems on both façades.

4.6 Adjusting the Significance of Sustainability Factors

In all the results presented in the previous sections, it was assumed that all three objective functions are equally important in the optimization process. However, when it comes to installing PV systems on façades, perspectives can differ. For example, project owners or stakeholders may prioritize economic aspects over environmental and energy-sufficiency considerations, leading to different priorities in the optimization process. This section aims to investigate the effect of assigning different weights to the objective functions as a post-processing step, similar to a multi-criteria decision-making (MCDM) approach. By doing so, we can explore how the final PV layout might change when the focus of the optimization is adjusted. Due to computational reasons and the interdependencies between the optimization of west and east façade orientations with the selected optimized PV system for the south façade, we will only examine this effect on the south façade of the CSC building. The goal is to emphasize the significance of considering various weights for the objective functions and how it can influence the selection of the optimal PV layout. This analysis provides valuable insights into the decision-making process and highlights the importance of balancing different sustainability aspects in the optimization process.

Following the optimization process with the Wallacei plugin, the objective function values for all solutions in the population are saved. MCDM can be conducted by normalizing these values, multiplying them by coefficients, and then adding them to determine the minimum amount. Similar to the optimization process, the values of the SS function are multiplied by -1 since the goal is to maximize it. The coefficients, denoted as a , b , and c , are considered to determine the importance of each energy efficiency, economic, and environmental parameter respectively. Each layout with specific PV design settings can be treated as an alternative in the decision-making process. In this section, a comparison of seven different sets of coefficients is presented to analyze their effects on

the module arrangement in the PV system. Table 13 and Table 14 display the PV layout parameters, encompassing the optimized variables and the total count of PV panels for the south façade of the CSC building under different scenarios. Furthermore, Figure 28 visually presents the various PV arrangements on the south façade of the CSC building corresponding to each scenario.

Table 13. PV system design parameters for the south façade of CSC building under different scenarios

	Scenarios			PV parameters					
	<i>a</i>	<i>b</i>	<i>c</i>	L_h	L_v	β	γ	r	N
(1)	0.33	0.33	0.33	0.0 m	3.0 m	40°	0°	90°	34
(2)	1	0	0	0.0 m	1.0 m	0°	0°	90°	154
(3)	0	1	0	0.0 m	3.0 m	40°	0°	135°	10
(4)	0	0	1	0.0 m	3.0 m	40°	0°	135°	10
(5)	0	0.5	0.5	0.0 m	3.0 m	40°	0°	135°	10
(6)	0.5	0	0.5	0.0 m	0.0 m	10°	0°	90°	110
(7)	0.5	0.5	0	0.0 m	0.0 m	10°	0°	90°	110

Table 14. Achieved objective values for south façade of CSC building in various scenarios

	Scenarios			Objective functions		
	<i>a</i>	<i>b</i>	<i>c</i>	SS	PB	$GHGE_{rate}$
(1)	0.33	0.33	0.33	6.03%	24	11.98
(2)	1	0	0	14.17%	41	20.78
(3)	0	1	0	1.98%	22	11.15
(4)	0	0	1	1.98%	22	11.15
(5)	0	0.5	0.5	1.98%	22	11.15
(6)	0.5	0	0.5	13.44%	32	15.94
(7)	0.5	0.5	0	13.44%	32	15.94

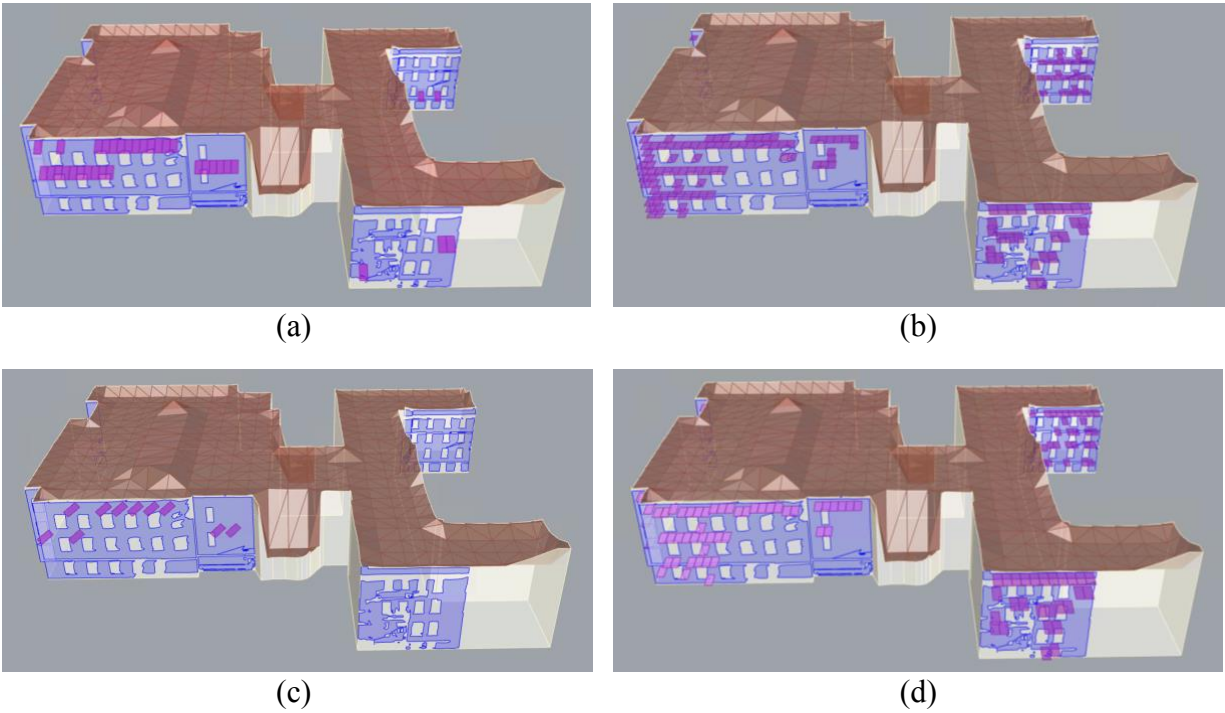


Figure 28. PV system configurations in different scenarios: (a) Scenario #1; (b) Scenario #2; (c) Scenarios #3, #4, & #5; (d) Scenarios #6 & #7

Based on the presented findings, in scenario #2 where the optimization prioritizes SS , the highest number of PV panels, 154 in total, is installed, resulting in an annual electrical energy production of 43436.31 kWh. Additionally, this scenario exhibits the highest PB of 41 years and $GHGE_{rate}$ of 20.78 g CO₂-eq./kWh. This indicates that the optimization process primarily aims to maximize the number of panels installed on the wall areas without significant consideration for other factors. Interestingly, scenarios #3 (emphasizing solely the economic perspective), #4 (prioritizing the environmental aspect exclusively), and #5 (giving equal importance to both economic and environmental aspects while disregarding energy efficiency) yield identical results with the lowest number of panels (10) generating 5257.81 kWh energy. This suggests that in the minimization of $GHGE_{rate}$ and PB , the optimization focuses on placing high-performing panels with minimal shading impact (as depicted in the figure above) and maximizing electricity generation. As

anticipated, PB and $GHGE_{rate}$ show the lowest values in these scenarios, with PB at 22 years and $GHGE_{rate}$ at 11.15 g CO₂-eq./kWh, respectively. Lastly, in scenario #6, where energy efficiency and environmental aspects are equally significant, while the economic aspect is disregarded, and scenario #7, where energy efficiency and economic aspects are equally important, while the environmental aspect is disregarded, the results are also identical, with 110 solar panels collectively generating 40434.57 kWh of energy per year. Having a SS of 13.44%, PB of 32 years and $GHGE_{rate}$ of 15.94 g CO₂-eq./kWh, this particular solution falls between the values obtained for the other two previously discussed scenarios.

4.7 Discussion & Recommendations

Typically, in the northern hemisphere, solar panels placed facing south tend to generate more electricity [75], [87], [89], and this observation is evident in the results of the PV placement optimization for both case study buildings. For the west façades of both buildings, the azimuth angle ranges between 30° and 60°, suggesting a southwest orientation for PV panels. This orientation is logical considering the shading effects caused by the façade surfaces. Similarly, for the east façade, the azimuth angle of the optimal layout is -30°, indicating a southeast orientation for PV panels.

The optimal tilt angles for the PV layouts of all case study façades fall within the range of 40° to 60°. This aligns with previous research [97], [98], which indicates that setting the tilt angle at approximately $\pm 10^\circ$ of the region's latitude is ideal for PV installations. As Edmonton's latitude is around 50°, the observed tilt angles in this study are consistent with the recommended optimal angles for maximizing solar energy generation in this region.

The horizontal distance of the optimized PV layouts ranges from 0.0 m to 0.5 m, while the vertical distance also falls within this range, except for one instance, which is the south façade of the CSC building. In this case, the vertical distance might differ due to the presence of multiple trees located in close proximity to the south façade faces of the building, resulting in shading effects that impact the PV panel placements.

The discrepancy in the total number of optimized PV panels between the CSC building (131 panels) and the NW-VVC building (209 panels), along with the higher energy demand of CSC compared to NW-VVC, logically results in a lower total SS for CSC compared to NW-VVC. Furthermore, the PB and $GHGE_{rate}$ of CSC are higher than those of NW-VVC. This difference could be attributed to the presence of more obstructions and surrounding objects near the CSC façades, which may increase the shading effect on solar panels and reduce their performance efficiency, ultimately leading to a lower amount of energy being produced. It is worth mentioning that we consider the initial energy demand of the building before the placement of optimal PV systems when reporting the final objective values. This choice is based on the fact that the variation in total energy demand of the buildings after implementing the optimal PV systems was approximately 0.5% higher than the pre-PV placement demand.

The findings from the "Adjusting the Significance of Sustainability Factors" section highlight that the optimized layout is influenced by the relative importance given to the objective functions. It is important to note that this section is a post-processing step conducted after the main optimization process with the three primary objective functions: SS , PB , and $GHGE_{rate}$, is completed. This implies that if, for instance, stakeholders prioritize the economic aspect and consider only PB as the main objective function during the optimization, the final optimized solution may differ from the scenario where $a=0$, $b=1$, and $c=0$. When focusing solely on optimizing SS above other

objectives, the optimized solution favors a layout with the highest number of panels and the greatest generation capacity. Consequently, the PB and $GHGE_{rate}$ are also the highest compared to the other scenarios. Additionally, the tilt angle is adjusted to 0° so that there would be more room for the panels, indicating reduced emphasis on maximizing the individual panel's performance efficiency and minimizing its generation loss. On the contrary, when the optimization prioritizes minimizing the PB and emission rate, the resulting solution remains consistent across three scenarios: when solely focusing on minimizing PB (economic factor), solely minimizing emissions (environmental factor), or when both PB and $GHGE_{rate}$ are equally important while disregarding SS . In such cases, the optimized solution changes to the one with the most efficient panels with the highest generation output and minimal shading impact. Consequently, the number of panels is minimized, leading to the lowest PB and $GHGE_{rate}$ values compared to the other scenarios mentioned. The findings also suggest that the azimuth angle of PV panels is not notably influenced by the energy efficiency, economic or environmental considerations of the owners.

4.8 Limitations & Future Work

The current study has some limitations that should be acknowledged. Firstly, the optimization process may become time-consuming when dealing with larger PV installable areas, but this can be overcome by increasing computational power. Secondly, the CNN model employed for predicting façade elements might not provide precise predictions for regions obstructed by trees or vegetation, or for areas with a high density of diverse elements. Incorporating approaches from existing studies, such as adding a context aggregation branch or more training data, could improve the model's performance in such cases. Another constraint to consider is that in the devised method, all building meshes whose projections closely align with each edge of the building footprint are consolidated into a singular surface. As a result, the resulting surface may not provide a highly

precise representation of all the elements on the designated facade. Another limitation arises when the geometries of trees or other obstacles are closely intertwined with buildings, resulting in merged and indistinguishable building and tree meshes. This complicates the accurate simplification of building geometry in these regions. Nevertheless, it is generally recommended to steer clear of installing panels on heavily obscured parts of facades to mitigate substantial energy generation loss due to shading. Additionally, in areas where meshes from trees or other objects cannot be separated, certain meshes shared by both geometries are exclusively factored into the building simplification process, exempted from being treated as obstacles in the shading analysis section of the algorithm. Considering each façade orientation separately in the current work was necessary to manage the complexity of the optimization process. Future research could explore techniques to simultaneously optimize PV solutions for all façades together, expanding the search space efficiently. Another limitation relates to cases with multiple volume spaces of different heights in a building geometry, where the building simplification algorithm struggles to recreate accurate vertical faces at intersecting points. Future work can explore enhancements to address this issue. Another aspect to consider for future work is that the inclusion of other sustainability factors, including socio-political and regulatory perspectives, can also be instrumental in advancing the adoption of PV façade systems. This approach has similarly been explored in the application of PV for community initiatives [99]. It is important to highlight that the developed framework can be used not only for existing buildings but also for new construction projects, as long as we have access to the 3D model of the building, its footprint, and architectural designs of the façade. This aspect can be explored in future research endeavors. Lastly, the study assumes no storage system in the building, so extra generated energy exceeding the demand in certain hours

is not considered during the optimization process. Future studies may incorporate storage systems to better utilize surplus energy.

Chapter Five: Conclusion

To successfully integrate PV façade systems into sustainable building development, conducting a comprehensive sustainability assessment before implementation is crucial. This assessment should address the neglected challenge of automatically identifying the installable parts of façades for PV placement, which is an essential aspect in optimizing PV layouts for façades. Regrettably, many PV systems are often employed for symbolic purposes, overlooking their full potential in advancing sustainable construction practices. Rather than solely prioritizing the aesthetic aspects of PV façade integration, designers and engineers should emphasize the selection of sustainable PV modules, application types, and installation methods to achieve the ultimate goal of constructing zero-emission buildings.

This study presents a holistic optimization framework that considers energy efficiency, economic viability, and environmental factors in sustainable development when integrating PV panels into building façades. The self-sufficiency rate (SS), payback period (PB), and greenhouse gas emission rate ($GHGE_{rate}$) are utilized as measures of energy efficiency, economic viability, and environmental impact, respectively.

The procedure begins with importing 3D models of the buildings and simplifying their geometries. Then, a deep learning model is deployed to identify suitable areas for PV installation, with a primary focus on walls. Subsequently, annual hourly PV generation, considering shading effects from neighboring objects, buildings, trees, and other factors that may impact PV generation, and annual energy demand simulation models are established. To find the optimal PV system design parameters, such as tilt, azimuth, rotation angles, and the vertical and horizontal panel placement, an evolutionary multi-objective optimization engine is employed. To demonstrate the practical

application of this comprehensive framework, two buildings situated on the North Campus of the University of Alberta in Edmonton, Alberta, Canada, are chosen for its implementation.

The findings highlight the importance of adjusting the priorities of objectives, as it can lead to diverse optimized solutions. Therefore, the study emphasizes the significance of considering multiple factors during the design of PV systems for building façades, moving beyond mere aesthetic considerations and emphasizing the promotion of sustainable buildings. For instance, when the sole focus is on *SS*, the chosen solution changes to one with the highest number of panels and PV generation. However, maximizing the individual performance of the panels is disregarded in this case, as the selected solution shifts from the optimal tilt angle range to 0° , allowing for more panels to be installed. On the other hand, when stakeholders prioritize purely economic, purely environmental, or equally economic and environmental aspects, disregarding energy efficiency, the optimized solution remains the same for all these scenarios. This solution has the lowest number of panels, as well as the lowest *PB*, *GHGE_{rate}*, and *SS* values. The optimized solution resulting from this prioritization contains only the most high-performing panels, ensuring maximum generation capacity and minimal shading effects. The results also imply that the orientation (azimuth angle) of PV panels is not significantly influenced by the energy efficiency, economic, or environmental preferences of the owners.

In summary, the primary goal of this study is to offer a comprehensive framework that emphasizes the significance of integrating various sustainability aspects, such as economic, environmental, and energy efficiency factors, when implementing PV façade applications. Additionally, the importance of façade parsing, which aids in selecting the optimal façade elements for panel installation, is highlighted in the analysis. The proposed framework is applicable in any location, provided that the 3D Google Maps model and footprint of the building along with the

corresponding weather file (EPW) are available. As previously highlighted, the current study carries several limitations and opportunities for future research. For instance, managing larger PV areas within the optimization process can be time-consuming, and a potential solution lies in bolstering computational capabilities. The CNN model used for predicting façade elements may encounter difficulties in regions obstructed by trees, vegetation, or diverse elements, indicating potential improvements through context aggregation or the augmentation of training data. The decision to individually optimize each façade is attributed to the intricacies of the process, presenting avenues for future exploration of more streamlined simultaneous optimization across all façades. Notably, the study does not incorporate building energy storage, resulting in untapped surplus energy. Subsequent research could explore the integration of storage systems to enhance overall energy efficiency.

References

- [1] D. E. Attoye, K. A. T. Aoul, and A. Hassan, “A review on building integrated photovoltaic façade customization potentials,” *Sustainability (Switzerland)*, vol. 9, no. 12, 2017, doi: 10.3390/su9122287.
- [2] S. A. Sharif and A. Hammad, “Simulation-Based Multi-Objective Optimization of institutional building renovation considering energy consumption, Life-Cycle Cost and Life-Cycle Assessment,” *Journal of Building Engineering*, vol. 21, pp. 429–445, 2019, doi: 10.1016/j.jobe.2018.11.006.
- [3] M. W. Akram, M. Hasannuzaman, E. Cuce, and P. M. Cuce, “Global technological advancement and challenges of glazed window, facade system and vertical greenery-based energy savings in buildings: A comprehensive review,” *Energy and Built Environment*, vol. 4, no. 2, pp. 206–226, 2023, doi: 10.1016/j.enbenv.2021.11.003.
- [4] S. Yip, A. K. Athienitis, and B. Lee, “Early stage design for an institutional net zero energy archetype building. Part 1: Methodology, form and sensitivity analysis,” *Solar Energy*, vol. 224, no. October 2019, pp. 516–530, 2021, doi: 10.1016/j.solener.2021.05.091.
- [5] A. Kumar Behura, A. Kumar, D. Kumar Rajak, C. I. Pruncu, and L. Lamberti, “Towards better performances for a novel rooftop solar PV system,” *Solar Energy*, vol. 216, no. January, pp. 518–529, 2021, doi: 10.1016/j.solener.2021.01.045.
- [6] F. Mansouri Kouhestani, J. Byrne, D. Johnson, L. Spencer, P. Hazendonk, and B. Brown, “Evaluating solar energy technical and economic potential on rooftops in an urban setting: the city of Lethbridge, Canada,” *International Journal of Energy and Environmental*

- Engineering*, vol. 10, no. 1, pp. 13–32, Mar. 2019, doi: 10.1007/S40095-018-0289-1/TABLES/10.
- [7] “Solar resource maps and GIS data for 200+ countries | Solargis.” <https://solargis.com/maps-and-gis-data/download/canada> (accessed Jul. 17, 2021).
- [8] T. E. Kuhn, C. Erban, M. Heinrich, J. Eisenlohr, F. Ensslen, and D. H. Neuhaus, “Review of technological design options for building integrated photovoltaics (BIPV),” *Energy Build*, vol. 231, p. 110381, 2021, doi: 10.1016/j.enbuild.2020.110381.
- [9] H. Awad, M. Gül, and M. Al-Hussein, “Long-term performance and GHG emission offset analysis of small-scale grid-tied residential solar PV systems in northerly latitudes,” *Advances in Building Energy Research*, vol. 15, no. 6, pp. 733–754, 2021, doi: 10.1080/17512549.2020.1720812.
- [10] A. Ghosh, “Potential of building integrated and attached/applied photovoltaic (BIPV/BAPV) for adaptive less energy-hungry building’s skin: A comprehensive review,” *J Clean Prod*, vol. 276, p. 123343, 2020, doi: 10.1016/j.jclepro.2020.123343.
- [11] Y. Lu, R. Chang, V. Shabunko, and A. T. Lay Yee, “The implementation of building-integrated photovoltaics in Singapore: drivers versus barriers,” *Energy*, vol. 168, pp. 400–408, 2019, doi: 10.1016/j.energy.2018.11.099.
- [12] S. Freitas and M. C. Brito, “Solar façades for future cities,” *Renewable Energy Focus*, vol. 31, no. December, pp. 73–79, 2019, doi: 10.1016/j.ref.2019.09.002.

- [13] D. E. Attoye, K. A. T. Aoul, and A. Hassan, “A review on building integrated photovoltaic façade customization potentials,” *Sustainability (Switzerland)*, vol. 9, no. 12, 2017, doi: 10.3390/su9122287.
- [14] P. Jayathissa, M. Luzzatto, J. Schmidli, J. Hofer, Z. Nagy, and A. Schlueter, “Optimising building net energy demand with dynamic BIPV shading,” *Appl Energy*, vol. 202, pp. 726–735, 2017, doi: 10.1016/j.apenergy.2017.05.083.
- [15] H. K. Abdullah and H. Z. Alibaba, “Retrofits for energy efficient office buildings: Integration of optimized photovoltaics in the form of responsive shading devices,” *Sustainability (Switzerland)*, vol. 9, no. 11, 2017, doi: 10.3390/su9112096.
- [16] Y. Sun *et al.*, “Integrated semi-transparent cadmium telluride photovoltaic glazing into windows: Energy and daylight performance for different architecture designs,” *Appl Energy*, vol. 231, no. June, pp. 972–984, 2018, doi: 10.1016/j.apenergy.2018.09.133.
- [17] C. Liu, W. Xu, A. Li, D. Sun, and H. Huo, “Analysis and optimization of load matching in photovoltaic systems for zero energy buildings in different climate zones of China,” *J Clean Prod*, vol. 238, p. 117914, 2019, doi: 10.1016/j.jclepro.2019.117914.
- [18] C. Liu, W. Xu, A. Li, D. Sun, and H. Huo, “Energy balance evaluation and optimization of photovoltaic systems for zero energy residential buildings in different climate zones of China,” *J Clean Prod*, vol. 235, pp. 1202–1215, 2019, doi: 10.1016/j.jclepro.2019.07.008.
- [19] M. Li *et al.*, “Numerical and experimental investigation of precast concrete facade integrated with solar photovoltaic panels,” *Appl Energy*, vol. 253, no. March, p. 113509, 2019, doi: 10.1016/j.apenergy.2019.113509.

- [20] Y. Cheng, M. Gao, J. Jia, Y. Sun, Y. Fan, and M. Yu, “An optimal and comparison study on daylight and overall energy performance of double-glazed photovoltaics windows in cold region of China,” *Energy*, vol. 170, pp. 356–366, 2019, doi: 10.1016/j.energy.2018.12.097.
- [21] C. sung Lee, H. Lee, M. Choi, and J. Yoon, “Design optimization and experimental evaluation of photovoltaic double skin facade,” *Energy Build*, vol. 202, p. 109314, 2019, doi: 10.1016/j.enbuild.2019.07.031.
- [22] E. Taveres-cachat, G. Lobaccaro, F. Goia, and G. Chaudhary, “A methodology to improve the performance of PV integrated shading devices using multi-objective optimization,” *Appl Energy*, vol. 247, no. March, pp. 731–744, 2019, doi: 10.1016/j.apenergy.2019.04.033.
- [23] X. Chen, H. Yang, and J. Peng, “Energy optimization of high-rise commercial buildings integrated with photovoltaic facades in urban context,” *Energy*, vol. 172, pp. 1–17, 2019, doi: 10.1016/j.energy.2019.01.112.
- [24] N. Skandalos and J. Tywoniak, “Influence of PV facade configuration on the energy demand and visual comfort in office buildings Influence of PV facade configuration on the energy demand and visual comfort in office buildings,” pp. 0–6, 2019, doi: 10.1088/1742-6596/1343/1/012094.
- [25] H. Alrashidi, A. Ghosh, W. Issa, N. Sellami, T. K. Mallick, and S. Sundaram, “Thermal performance of semitransparent CdTe BIPV window at temperate climate,” *Solar Energy*, vol. 195, no. December 2019, pp. 536–543, 2020, doi: 10.1016/j.solener.2019.11.084.

- [26] A. Mesloub, G. A. Albaqawy, and M. Z. Kandar, “The optimum performance of Building Integrated Photovoltaic (BIPV) Windows under a semi-arid climate in Algerian Office Buildings,” *Sustainability (Switzerland)*, vol. 12, no. 4, 2020, doi: 10.3390/su12041654.
- [27] A. Mesloub, A. Ghosh, M. Touahmia, G. A. Albaqawy, E. Noaime, and B. M. Alsolami, “Performance analysis of photovoltaic integrated shading devices (Pvsds) and semi-transparent photovoltaic (stpv) devices retrofitted to a prototype office building in a hot desert climate,” *Sustainability (Switzerland)*, vol. 12, no. 23, pp. 1–18, 2020, doi: 10.3390/su122310145.
- [28] P. Florio, G. Peronato, A. T. D. Perera, A. Di Blasi, K. H. Poon, and J. H. Kämpf, “Designing and assessing solar energy neighborhoods from visual impact,” *Sustain Cities Soc*, vol. 71, 2021, doi: 10.1016/j.scs.2021.102959.
- [29] H. S. Choi, “Architectural Experiment Design of Solar Energy Harvesting: A Kinetic Façade System for Educational Facilities,” *Applied Sciences*, vol. 12, no. 12, p. 5853, 2022, doi: 10.3390/app12125853.
- [30] X. Feng, T. Ma, Y. Yamaguchi, J. Peng, Y. Dai, and D. Ji, “Potential of residential building integrated photovoltaic systems in different regions of China,” *Energy for Sustainable Development*, vol. 72, no. December 2022, pp. 19–32, 2023, doi: 10.1016/j.esd.2022.11.006.
- [31] L. Lu and H. X. Yang, “Environmental payback time analysis of a roof-mounted building-integrated photovoltaic (BIPV) system in Hong Kong,” *Appl Energy*, vol. 87, no. 12, pp. 3625–3631, 2010, doi: 10.1016/j.apenergy.2010.06.011.

- [32] H. Gholami and H. N. Røstvik, “Economic analysis of BIPV systems as a building envelope material for building skins in Europe,” *Energy*, vol. 204, p. 117931, 2020, doi: 10.1016/j.energy.2020.117931.
- [33] F. Vahdatikhaki, N. Salimzadeh, and A. Hammad, “Optimization of PV modules layout on high-rise building skins using a BIM-based generative design approach,” *Energy Build*, vol. 258, p. 111787, 2022, doi: 10.1016/j.enbuild.2021.111787.
- [34] M. J. Sorgato, K. Schneider, and R. Rütther, “Technical and economic evaluation of thin-film CdTe building-integrated photovoltaics (BIPV) replacing façade and rooftop materials in office buildings in a warm and sunny climate,” *Renew Energy*, vol. 118, pp. 84–98, 2018, doi: 10.1016/j.renene.2017.10.091.
- [35] T. Mendis, Z. Huang, and S. Xu, “Determination of economically optimised building integrated photovoltaic systems for utilisation on facades in the tropical climate: A case study of Colombo, Sri Lanka,” *Build Simul*, vol. 13, no. 1, pp. 171–183, 2020, doi: 10.1007/s12273-019-0579-4.
- [36] R. Elghamry, H. Hassan, and A. A. Hawwash, “A parametric study on the impact of integrating solar cell panel at building envelope on its power, energy consumption, comfort conditions, and CO₂ emissions,” *J Clean Prod*, vol. 249, p. 119374, 2020, doi: 10.1016/j.jclepro.2019.119374.
- [37] M. K. Ansah and X. Chen, “Two-Stage Lifecycle Energy Optimization of Mid-Rise Residential Buildings with Building-Integrated Photovoltaic and Alternative Composite Façade Materials,” 2021.

- [38] Y. Kurdi, B. J. Alkhatatbeh, S. Asadi, and H. Jebelli, “A decision-making design framework for the integration of PV systems in the urban energy planning process,” *Renew Energy*, vol. 197, no. June, pp. 288–304, 2022, doi: 10.1016/j.renene.2022.07.001.
- [39] Z. Liu *et al.*, “A comprehensive study of feasibility and applicability of building integrated photovoltaic (BIPV) systems in regions with high solar irradiance,” *J Clean Prod*, vol. 307, no. May, p. 127240, 2021, doi: 10.1016/j.jclepro.2021.127240.
- [40] E. Hadi and A. Heidari, “Development of an integrated tool based on life cycle assessment, Levelized energy, and life cycle cost analysis to choose sustainable Facade Integrated Photovoltaic Systems,” *J Clean Prod*, vol. 293, p. 126117, 2021, doi: 10.1016/j.jclepro.2021.126117.
- [41] G. Nishida, A. Bousseau, and D. G. Aliaga, “Procedural Modeling of a Building from a Single Image,” 2018.
- [42] H. Liu, Y. Xu, J. Zhang, J. Zhu, Y. Li, and S. C. H. Hoi, “DeepFacade: A Deep Learning Approach to Facade Parsing with Symmetric Loss,” *IEEE Trans Multimedia*, vol. 22, no. 12, pp. 3153–3165, 2020, doi: 10.1109/TMM.2020.2971431.
- [43] C. K. Li, H. X. Zhang, J. X. Liu, Y. Q. Zhang, S. C. Zou, and Y. T. Fang, “Window Detection in Facades Using Heatmap Fusion,” *J Comput Sci Technol*, vol. 35, no. 4, pp. 900–912, 2020, doi: 10.1007/s11390-020-0253-4.
- [44] W. Ma, S. Xu, W. Ma, and H. Zha, “Multiview Feature Aggregation for Facade Parsing,” *IEEE Geoscience and Remote Sensing Letters*, vol. 19, 2022, doi: 10.1109/LGRS.2020.3035721.

- [45] H. Liu, W. Li, and J. Zhu, “Translational Symmetry-Aware Facade Parsing for 3D Building Reconstruction,” pp. 1–12, 2021, [Online]. Available: <http://arxiv.org/abs/2106.00912>
- [46] N. Nordmark and M. Ayenew, “Window Detection In Facade Imagery: A Deep Learning Approach Using Mask R-CNN,” no. 2007, 2021, [Online]. Available: <http://arxiv.org/abs/2107.10006>
- [47] W. Ma, W. Ma, S. Xu, and H. Zha, “Pyramid ALKNet for Semantic Parsing of Building Facade Image,” *IEEE Geoscience and Remote Sensing Letters*, vol. 18, no. 6, pp. 1009–1013, Jun. 2021, doi: 10.1109/LGRS.2020.2993451.
- [48] W. Ma, S. Xu, W. Ma, X. Zhang, and H. Zha, “Progressive Feature Learning for Facade Parsing with Occlusions,” *IEEE Transactions on Image Processing*, vol. 31, pp. 2081–2093, 2022, doi: 10.1109/TIP.2022.3152004.
- [49] W. Ma, W. Ma, and S. Xu, “Deep Facade Parsing with Occlusions,” *KSII Transactions on Internet and Information Systems*, vol. 16, no. 2, pp. 524–543, Feb. 2022, doi: 10.3837/tiis.2022.02.009.
- [50] G. Zhang, Y. Pan, and L. Zhang, “Deep learning for detecting building façade elements from images considering prior knowledge,” *Autom Constr*, vol. 133, Jan. 2022, doi: 10.1016/j.autcon.2021.104016.
- [51] “RenderDoc.” <https://renderdoc.org/> (accessed Jul. 01, 2022).
- [52] “blender.org - Home of the Blender project - Free and Open 3D Creation Software.” <https://www.blender.org/> (accessed Jul. 14, 2022).

- [53] “GitHub - eliemichel/MapsModelsImporter: A Blender add-on to import models from google maps.” <https://github.com/eliemichel/MapsModelsImporter> (accessed Jul. 14, 2022).
- [54] “Rhino - Rhinoceros 3D.” <https://www.rhino3d.com/> (accessed Aug. 03, 2022).
- [55] “Edmonton - Open Data Portal.” <https://data.edmonton.ca/> (accessed Aug. 03, 2022).
- [56] “Building Footprint | Edmonton - Open Data Portal.” <https://data.edmonton.ca/Geospatial-Boundaries/Building-Footprint/6n9r-ddf8> (accessed Jun. 03, 2023).
- [57] “Welcome to the QGIS project!” <https://qgis.org/en/site/> (accessed Aug. 03, 2022).
- [58] “Rhino - Features.” <https://www.rhino3d.com/features/#grasshopper> (accessed Aug. 03, 2022).
- [59] “Most Used Grasshopper Plugins for Architects - Archgyan.” <https://archgyan.com/blog/most-used-grasshopper-plugins-for-architects/> (accessed Aug. 03, 2022).
- [60] F. Kor and W. Förstner, “eTRIMS Image Database for Interpreting Images of Man-Made Scenes,” 2009.
- [61] R. Gadde, R. Marlet, and N. Paragios, “Learning Grammars for Architecture-Specific Facade Parsing,” *Int J Comput Vis*, vol. 117, no. 3, pp. 290–316, May 2016, doi: 10.1007/S11263-016-0887-4/FIGURES/15.
- [62] “CMP Facade Database.” <https://cmp.felk.cvut.cz/~tylecr1/facade/> (accessed Sep. 05, 2022).

- [63] “Labelbox | The Leading AI Platform for Building Intelligent Applications.”
<https://labelbox.com/> (accessed Aug. 19, 2022).
- [64] “GitHub - SunYW0108/DeepWindows: PyTorch Implementation of DeepWindows.”
<https://github.com/SunYW0108/DeepWindows> (accessed Sep. 05, 2022).
- [65] Y. Sun, S. Malihi, H. Li, and M. Maboudi, “DeepWindows: Windows Instance Segmentation through an Improved Mask R-CNN Using Spatial Attention and Relation Modules,” *ISPRS International Journal of Geo-Information* 2022, Vol. 11, Page 162, vol. 11, no. 3, p. 162, Feb. 2022, doi: 10.3390/IJGI11030162.
- [66] L. C. Chen, Y. Zhu, G. Papandreou, F. Schroff, and H. Adam, “Encoder-Decoder with Atrous Separable Convolution for Semantic Image Segmentation,” *Lecture Notes in Computer Science (including subseries Lecture Notes in Artificial Intelligence and Lecture Notes in Bioinformatics)*, vol. 11211 LNCS, pp. 833–851, Feb. 2018, doi: 10.1007/978-3-030-01234-2_49.
- [67] “Anaconda | The World’s Most Popular Data Science Platform.”
<https://www.anaconda.com/> (accessed Sep. 07, 2022).
- [68] “Project Jupyter | Home.” <https://jupyter.org/> (accessed Sep. 07, 2022).
- [69] “GitHub - albuumentations-team/albuumentations: Fast image augmentation library and an easy-to-use wrapper around other libraries. Documentation: <https://albuumentations.ai/docs/> Paper about the library: <https://www.mdpi.com/2078-2489/11/2/125>.”
<https://github.com/albuumentations-team/albuumentations> (accessed Sep. 24, 2022).

- [70] A. Buslaev, V. I. Iglovikov, E. Khvedchenya, A. Parinov, M. Druzhinin, and A. A. Kalinin, “Albumentations: Fast and flexible image augmentations,” *Information (Switzerland)*, vol. 11, no. 2, Feb. 2020, doi: 10.3390/INFO11020125.
- [71] “GitHub - qubvel/segmentation_models.pytorch: Segmentation models with pretrained backbones. PyTorch.” https://github.com/qubvel/segmentation_models.pytorch (accessed Sep. 20, 2022).
- [72] “patchify · PyPI.” <https://pypi.org/project/patchify/> (accessed Sep. 23, 2022).
- [73] “Google Earth.” <https://earth.google.com/web/@0,-7.3288999,0a,22251752.77375655d,35y,0h,0t,0r> (accessed Nov. 09, 2022).
- [74] “ShapeDiver | Cloud applications for Grasshopper.” <https://shapediver.com/> (accessed Apr. 09, 2023).
- [75] J. A. Duffie and W. A. Beckman, “Solar Engineering of Thermal Processes: Fourth Edition,” *Solar Engineering of Thermal Processes: Fourth Edition*, Apr. 2013, doi: 10.1002/9781118671603.
- [76] “HiKu – Canadian Solar – Global.” <https://www.canadiansolar.com/hiku/> (accessed Apr. 09, 2023).
- [77] “CS3W-420P solar panel from Canadian Solar: specs, prices and reviews.” <https://www.solarreviews.com/manufacturers/canadian-solar/solar-panels/canad49988hikucs3w420p> (accessed Apr. 09, 2023).
- [78] M. S. Roudsari and M. Pak, “Ladybug: A parametric environmental plugin for grasshopper to help designers create an environmentally-conscious design,” *Proceedings of BS 2013:*

13th Conference of the International Building Performance Simulation Association, pp. 3128–3135, 2013.

- [79] “Ladybug Tools | Home Page.” <https://www.ladybug.tools/> (accessed Apr. 10, 2023).
- [80] “Radiance — Radsite.” <https://www.radiance-online.org/> (accessed Apr. 10, 2023).
- [81] “Annual Irradiance - HB-Radiance Primer.” https://docs.ladybug.tools/hb-radiance-primer/components/3_recipes/annual_irradiance (accessed Apr. 10, 2023).
- [82] “epwmap.” <https://www.ladybug.tools/epwmap/> (accessed Apr. 01, 2023).
- [83] T. Matthews and J. Sandercock, “Alternative Energy Program Solar Photovoltaic Reference Array Report,” p. 11, 2016, [Online]. Available: [https://solaralberta.ca/sites/default/files/NAIT Reference Array Report.pdf](https://solaralberta.ca/sites/default/files/NAIT%20Reference%20Array%20Report.pdf)
- [84] H. Awad, “Integrating Solar PV Systems into Residential Buildings in Cold-climate Regions : The Impact of Energy-efficient Homes on Shaping the Future Smart Grid,” 2018.
- [85] “Model to OSM - HB-Energy Primer.” https://docs.ladybug.tools/hb-energy-primer/components/5_simulate/model_to_osm (accessed Apr. 12, 2023).
- [86] “Solar Power Alberta (2021 Guide).” <https://www.energyhub.org/alberta/> (accessed Jul. 17, 2023).
- [87] N. Narjabadifam, “Optimizing rooftop solar PV systems in urban regions considering economic and environmental aspects,” 2022.
- [88] “Micro-Generation in Alberta – EnergyRates.ca.” <https://energyrates.ca/alberta/micro-generation-in-alberta/> (accessed Sep. 03, 2023).

- [89] N. Narjabadifam *et al.*, “Framework for Mapping and Optimizing the Solar Rooftop Potential of Buildings in Urban Systems,” *Energies* 2022, Vol. 15, Page 1738, vol. 15, no. 5, p. 1738, Feb. 2022, doi: 10.3390/EN15051738.
- [90] J. Peng, L. Lu, and H. Yang, “Review on life cycle assessment of energy payback and greenhouse gas emission of solar photovoltaic systems,” *Renewable and Sustainable Energy Reviews*, vol. 19. Elsevier Ltd, pp. 255–274, 2013. doi: 10.1016/j.rser.2012.11.035.
- [91] “Life Cycle Emissions Factors for Electricity Generation Technologies | NREL Data Catalog.” <https://data.nrel.gov/submissions/171> (accessed Jul. 18, 2023).
- [92] “Wallacei | About.” <https://www.wallacei.com/about> (accessed Apr. 20, 2023).
- [93] K. Deb, A. Pratap, S. Agarwal, and T. Meyarivan, “A fast and elitist multiobjective genetic algorithm: NSGA-II,” *IEEE Transactions on Evolutionary Computation*, vol. 6, no. 2, pp. 182–197, Apr. 2002, doi: 10.1109/4235.996017.
- [94] I. Elwy, Y. Ibrahim, M. Fahmy, and M. Mahdy, “Outdoor microclimatic validation for hybrid simulation workflow in hot arid climates against ENVI-met and field measurements,” *Energy Procedia*, vol. 153, pp. 29–34, Oct. 2018, doi: 10.1016/J.EGYPRO.2018.10.009.
- [95] M. Donato, G. Zemella, G. Rapone, J. Hussain, and C. Black, “An innovative app for a parametric, holistic and multidisciplinary approach to early design stages,” *Journal of Facade Design and Engineering*, vol. 5, no. 2, pp. 113–127, Dec. 2017, doi: 10.7480/JFDE.2017.2.1739.

- [96] A. Aksamija and L. A. Bd, “Methods for integrating parametric design with building performance analysis,” *ARCC Conference Repository*, Sep. 2018, doi: 10.17831/REP:ARCC.
- [97] H. Awad, K. M. E. Salim, and M. Gül, “Multi-objective design of grid-tied solar photovoltaics for commercial flat rooftops using particle swarm optimization algorithm,” *Journal of Building Engineering*, vol. 28, no. July 2019, p. 101080, 2020, doi: 10.1016/j.jobbe.2019.101080.
- [98] H. Awad and M. Gül, “Load-match-driven design of solar PV systems at high latitudes in the Northern hemisphere and its impact on the grid,” *Solar Energy*, vol. 173, pp. 377–397, Oct. 2018, doi: 10.1016/J.SOLENER.2018.07.010.
- [99] N. Narjabadifam, J. Fouladvand, and M. Gül, “Critical Review on Community-Shared Solar—Advantages, Challenges, and Future Directions,” *Energies 2023, Vol. 16, Page 3412*, vol. 16, no. 8, p. 3412, Apr. 2023, doi: 10.3390/EN16083412.